Observations and Modeling of Snow over the Washington Cascades

Hafen S. McCormick

A thesis submitted in partial fulfillment
of the requirements for the degree of

Master of Science

University of Washington

2009

Program Authorized to Offer Degree: Department of Atmospheric Sciences

University of Washington
Graduate School

This is to certify that I have examined this copy of a master's thesis by

Hafen S. McCormick

and have found that it is complete and satisfactory in all respects,
and that any and all revisions required by the final
examining committee have been made.

Committee Members:

_____
Robert A. Houze, Jr.

_____
Clifford F. Mass

_____
Mark T. Stoelinga

Date: _____

In presenting this thesis in partial fulfillment of the requirements for a master's degree at the University of Washington, I agree that the Library shall make its copies freely available for inspection. I further agree that extensive copying of this thesis is allowable only for scholarly purposes, consistent with "fair use" as prescribed in the U.S. Copyright Law. Any other reproduction for any purpose or by any means shall not be allowed without my written permission.

Signature_____

Date_____

TABLE OF CONTENTS

LIST OF FIGURES

LIST OF TABLES

Chapter 1

INTRODUCTION

1.1 Overview

The formation of precipitation within clouds involves a highly complex array of microphysical processes whereby water mass moves from the vapor phase onto collections of liquid or solid particles. These particles subsequently grow by a variety of processes until they become large enough to fall out and reach the ground as precipitation. The complexity of cloud microphysics arises from the shear number of particles involved, the wide variety of the particles' physical characteristics (such as size, shape, mass, and fall speed), and the many physical laws that govern how particles behave and grow. The study of cloud microphysics has a rich history that has led to an immense body of knowledge, and has filled several classic textbooks (e.g., Rogers and Yau, 1989; Young, 1993; Pruppacher and Klett, 1997). While the advancement of our understanding of cloud and precipitation microphysics is desirable from a purely scientific perspective, there is also the compelling practical motivation that accurate quantitative precipitation forecasts require an accurate representation of cloud and precipitation particles and their growth processes in numerical weather prediction (NWP) models.

The present study is designed to advance our knowledge in two specific areas of cloud microphysics, namely, the observed physical characteristics of snow particles, and the representation of snow particles within bulk cloud microphysical schemes used in NWP models.

There are compelling reasons to pay extra attention to the physical characteristics and growth of snow particles. First, snow particles are highly complex compared to

other liquid and solid hydrometeors of simpler form (e.g., cloud droplets, rain drops, hail stones). Individual snow particles grow through numerous processes that include deposition, riming, and aggregation. Further, those growth processes are influenced by changes in particle characteristics, yielding potentially complex feedbacks. The number of snow particles present at any given time is the result of both primary (ice nucleation) and secondary (e.g., rime-splintering (Hallett and Mossop, 1974)) ice particle formation mechanisms, as well as aggregation, all of which are complex processes that continue to spur active research. Finally, the effects of snow particle complexity and related processes are far-reaching, because for many important precipitation regimes, much of the precipitation mass reaching the ground began as snow. This is true of cold-season extratropical cyclonic storms, cold-cloud orographic precipitation, and stratiform precipitation associated with mesoscale convective systems.

For these reasons, the present study was carried out to increase our knowledge of snow particle variability and its implications for precipitation forecasting, with the following specific goals:

1. Gather a long-term observational data set over the course of two winter seasons in the Cascade Mountains, documenting the types of snow particles observed, their frequency, and other characteristics (such as fall speed and density).

2. Develop a climatology of observed precipitation in the Cascade Mountains by total mass fraction of different particle types, using established classification schemes for crystal habit type riming.

3. Use knowledge gained from the observational work for testing a recently developed method to predict snow particle habit type within a bulk microphysical scheme; and the development and testing of a new method to predict degree of riming of snow particles within a bulk scheme.

The next section provides background on the different growth processes for snow, how they affect snow particle type, and why snow particle type, in turn, affects the growth processes. Following that discussion are reviews of what other researchers have done in the areas of snow particle observational studies and representation of snow in bulk microphysical schemes, and why the present study is necessary to go beyond what those studies accomplished.

1.2 Background

1.2.1 Snow Growth Processes and Particle Types

After an ice crystal is nucleated, its initial growth occurs by deposition directly from the vapor phase. Deposition is affected by several factors. In the earliest stages of a crystal's growth, the manner in which deposition acts is dependent on the structure of the underlying nucleus. If the initial structure takes the form of a single lattice that is relatively free of defects, standard "monocrystals" are the result (e.g., planar dendrites, plates, columns). If the initial lattice structure is flawed, growth can occur along several randomly oriented crystal axes forming "polycrystals" (e.g., bullet rosettes, radiating assemblages of dendrites, radiating assemblages of plates, etc.).

Depositional growth is governed by both temperature and humidity, which determine not only the rate at which a crystal grows but also its "habit". Habit refers to the categorization of snow particles based on the characteristic shape of the particle. Temperature controls the preference for growth normal to either the prism faces (plate-like growth) or basal faces (columnar-like growth) of the crystal. Humidity is important in that ice saturation is required for any growth at all, and water saturation results in different habit types than what grows at the same temperature below water saturation (e.g., the transition from sectors to dendrites as water saturation is achieved).

The temperature and humidity can be locally affected by other factors such as

the degree of ventilation a crystal experiences or by its proximity to nearby cloud droplets. Since these conditions can vary greatly as a crystal moves through a cloud, a crystal's final shape is often quite complicated, having the characteristics of more than one habit.

When snow particles fall through clouds containing supercooled water, they collect droplets which then freeze on the particle, a process known as riming. The ability of any crystal to collide with and capture droplets is a function not only of its shape, but also of the its fall velocity relative to the collected droplets. As more and more droplets are captured, the particle density can increase as droplets fill in the open spaces within the crystal structure. The shape of the crystal is altered, eventually to the point that its habit-distinguishing features are obscured. This metamorphosis produces graupel-like snow, and finally, if riming continues, graupel. Riming generally accelerates growth through a positive feedback between the riming process, particle densification, and accelerated fall velocity. Other growth processes are affected as well by the change in particle characteristics, leading to complex feedbacks in the growth of precipitation.

Aggregation is the process whereby a larger snow particle collects smaller snow particles as it falls through them. The process leads to further complexity in particle structure, since the component particles may have been collected over a considerable depth of the atmosphere, and can therefore be of different habit types or degree of riming (although single habit-type aggregates are common as well). The growth of particles by aggregation leads to larger particles, but the aerodynamics of snow aggregates is such that large aggregates do not fall significantly faster than small aggregates or single crystals. Therefore, the aggregation process does not accelerate particle fallout nearly as much as growth of particles (either rain or snow) by collection of liquid water.

In an orographic setting, microphysical processes are complicated by issues of timing, as discussed by Smith (1979) and Smith and Barstad (2004). Mountains

cause disturbances in air flow, forcing windward assent and leeward descent. There is also evidence that turbulent cellularity associated with vertical sheer zones over mountains produces enhanced assent at small scales (Jr. and Medina, 2005). These vertical displacements first supply and then remove the moisture available for snow growth processes, over a timescale determined by the barrier width and the cross-barrier flow. The result is that the cloud system is sensitive to the rate at which precipitation growth processes occur, relative to the timescale of orographic assent. Therefore, in orographic environments in particular, the feedbacks between particle type, fall speed, and growth processes are likely to be more important than in other environments.

1.2.2 Ground-Based Observational Studies of Snow Particle Types

Several research groups have carried out extensive ground-based observations of snow particles. Of particular interest are those studies that included the identification of habit and especially those that also included the degree of riming. These field campaigns were carried out for a variety of purposes. Some were intended to support the evaluation of the feasibility of cloud seeding as a method for enhancing precipitation production (Hobbs, 1975; Rauber et al., 1986; Rauber and Grant, 1986; Super and Boe, 1988). Others were intended to provide insights into the microphysical structure aloft during precipitation events (Rauber, 1987; Sassen et al., 1990; Demoz et al., 1993). Still others were simply intended to measure the relationship between habit, possibly including riming, and various microphysically related quantities such as the particle mass (Locatelli and Hobbs, 1974; Mitchell et al., 1990), or fall velocity (Zikmunda, 1972; Locatelli and Hobbs, 1974; Barthazy and Schefolda, 2006) as a function of size, the number of fragments found in crystal-crystal collisions (Vardiman, 1978), and the density of freshly fallen snow (Power et al., 1964).

One of the more challenging aspects of snow particle observation studies is the identification of habit and degree of riming. For this reason, the choice of measure-

ment methodology is especially important. One method that has been used is to create photographs of snow particles (either with or without magnification) (Super and Boe, 1988; Mitchell et al., 1990; Demoz et al., 1993). A variation on this theme, known as shadow photography (Rauber et al., 1986; Rauber and Grant, 1986; Rauber, 1987; Sassen et al., 1990), had a light source placed at the bottom of a transparent box while snow particles were placed on top, with a film cartridge just millimeters above. While this method stored unmagnified images, it allowed for a reasonably magnified image to be projected. Another method commonly employed was to actually catch particles in a gelatinous substance called Formvar, leaving a permanent impression that could be examined later under a microscope (Power et al., 1964; Zikmunda, 1972; Hobbs, 1975; Barthazy and Schefolda, 2006). All these methods had the obvious advantage of being able to record data for later study, allowing for a potentially very detailed analysis. These methods also allowed for the possibility of automating the data collection process (Power et al., 1964; Vardiman, 1978). The primary drawbacks of all these methods are that they did not allow for manipulation of the sample when the image or impression was unclear or when important features were obscured. Additionally, they did not produce a detailed 3-D view. In contrast, the direct observation of particles under a stereo microscope (Locatelli and Hobbs, 1974; Vardiman, 1978) lent flexibility to the examination of the samples and allowed for a detailed 3-D view, which is often a necessary capability to distinguish certain habit types. Of course this method also had its disadvantages, namely keeping the samples cool long enough to make observations, having to do the analysis immediately, which potentially limited the number of observations that could be made over a fixed period of time, and having no permanent record of the samples' visual representation.

Aside from particle type, the two quantities whose measurement has received the most attention are the mass and fall speed of particles. These measurements are most useful when made in conjunction with particle size and type, so that relationships among these parameters can be developed. Particle mass has been measured only by

careful collection and melting of individual particles, and then measuring the melted drop size, which can be directly related to particle mass (Locatelli and Hobbs, 1974; Heymsfield, 1975; Kajikawa, 1989; Mitchell et al., 1990). In our studies we chose not to devote manpower to this laborious task, in favor of making a more comprehensive effort toward detailed assessment of habit types.

Most studies attempting to obtain velocity-diameter relationships with respect to habit did so one particle at a time. This meant the particle whose fall speed was being measured was also the particle whose habit was being identified. Commonly, the fall velocity was measured by means of high speed photography (Brown, 1970; Yagi, 1970; Zikmunda, 1972) in which regularly timed photos were quickly taken of a falling particle. The photos were subsequently analyzed, noting the distance the particle fell during each interval, and from this the fall velocity was calculated. When identifying the habit type of the particle, they relied upon the photographs (Brown, 1970; Yagi, 1970) or used Formvar (Zikmunda, 1972). These methodologies limited the number of crystals that could be measured and the detail with which habits could be identified. A variation on this theme (Locatelli and Hobbs, 1974) used two horizontally pointing, parallel beams of light, one above the other, so that as a falling crystal successively disrupted the beams, the time could be noted, and from this the fall velocity calculated. The measured particle would then be caught and identified under a microscope. Though this method of identification limited the rate of sampling further, it had the advantage of increasing the detail with which habits could be identified.

In contrast, more recent studies (Hanesch, 1999; Barthazy and Schefolda, 2006) have attempted to obtain fall velocity data on a much larger scale. To do this, habit identification was done on a representative sample of snow particles rather than on the particles whose fall speeds were actually measured. Separating the observations in this way enabled the fall speeds of large numbers of particles to be measured automatically by a 2-D video disdrometer (described in section 2.1.2). This methodology

was unable to relate the habit type of individual particles to their fall velocity, but it was able to relate the habit composition of the larger population to its overall velocity-diameter relationship. Though these studies increased the number of particles measured, they sacrificed the detail available to habit identification by using Formvar impressions. Barthazy and Schefolda (2006), for example, classified 83% of their slides as predominantly "irregular". Further, these studies limited the number of habit categories, with Hanesch (1999) using five and Barthazy and Schefolda (2006) using three. Barthazy and Schefolda (2006) also used only four of the six categories of riming described by Mosimann (1995). They also tended to record a dominant habit type rather than percentages of different habit types, with "dominant" being loosely defined (e.g., in the case of Barthazy, they required only that the habit type in question comprise at least 50% or more of the particles present).

Previous studies have focused on obtaining relationships between fall velocity and several other quantities. From these studies, we know that fall velocity varies with habit (Brown, 1970; Yagi, 1970; Locatelli and Hobbs, 1974). We also know that fall velocity increases with increasing size (Zikmunda, 1972; Locatelli and Hobbs, 1974) as well as with increasing mass (Locatelli and Hobbs, 1974). Further, for a given diameter, fall velocity increases with increasing density (Locatelli and Hobbs, 1974). This is particularly relevant to the process of riming since it tends to increase the mass of a crystal without changing its diameter. Also for a given diameter, there appears to be a large variance in fall velocities (Barthazy and Schefolda, 2006). In addition to documenting observed relationships between fall velocity and various other quantities, these studies have provided simple but useful power-law approximations of the velocity-diameter relationship, which have been used widely in NWP models due to their desirable mathematical properties.

In summary, studies that have attempted to relate particle habit to other quantities have used a variety of measurement methodologies to accomplish their goals. Some of these methodologies have emphasized the detailed observation of individual

particles and their characteristics. Others have focused on acquiring statistics on the bulk properties of precipitation by acquiring very large samples. In both cases, one aim was typically sacrificed in pursuit of the other. Our goal in the observational effort is to gather a data set that measures some quantities with more of a bulk approach (e.g., continuous 2-D video disdrometer measurements of particle size and fall speed, or continuous precipitation rate and snow depth measurements), but simultaneously captures detailed observations of a smaller (but representative) sample of the structural characteristics (habit and degree of riming) of falling snow particles. An additional goal is to gather that data set nearly continuously over multiple seasons, to maximize the variety of particles seen, and to quantify the climatology of particle types.

1.2.3 Microphysics Scheme

The primary way by which modern NWP models represent clouds and precipitation is through bulk microphysical schemes, which separately predict the mixing ratios of multiple classes of hydrometeor types. Schemes range in sophistication from those that model precipitation as warm rain (treating vapor, cloud water and rain water only) to those that are mixed-phase and have up to six different classes of water mass (e.g., vapor, cloud water, rain water, snow, and graupel or hail). The use of two species, snow and graupel, for the frozen precipitation mass is a common choice in typical modern bulk schemes. However, these two categories of hydrometeor are used to represent what, in nature, is a full spectrum of both shapes and degrees of riming for the frozen hydrometeors. Graupel, made up almost entirely of rime mass, varies only moderately in shape in nature. Snow on the other hand, a product of deposition in different habits and possibly varying degrees of riming, can take on a broad spectrum of shapes and densities. Yet many bulk schemes (Lin et al., 1983; Reisner et al., 1998; Hong et al., 2004; Thompson et al., 2004) represent snow as simple spheres of constant density. In other words, no adjustment to the physical

behavior of snow is made based on its growth history.

A few recent studies have made some effort to improve this situation. In one such effort (Thompson et al., 2008), the assumption that all snow particles are spheres of constant density was improved by replacing the cubed mass-diameter relationship with a more realistic squared one. Though improving the representation of snow's behavior, it retained the fixed nature of the mass-diameter relationship, preventing it from responding to changing environmental conditions and the growth history of the particles. More sophisticated strategies for improving the modeling of snow particles centered around making snow behavior sensitive to its shape. In particular, some have attempted to predict the mass of several different snow species (Straka and Mansell, 2005; Lynn et al., 2005). However, in these schemes, this was applied only to initial ice particles prior to aggregation. Aggregates of snow particles, which have been shown to dominate size spectra evolution in observed stratiform precipitation events (Houze et al., 1979; Lo and Passarelli, 1982; Mitchell, 1988; Ryan, 2000; Field and Heymsfield, 2003; Field et al., 2005), were still represented in these schemes by constant-density spheres. Thus, as soon as mass was transferred from the single-crystal ice categories to the snow aggregate category, which occurred on a fairly short time scale, no habit information was available to set habit-specific parameters, and the aggregate category was subject to the pitfalls of the constant-density sphere assumption. Another approach was that of (Meyers et al., 1997), who diagnosed (rather than predicted) the habit of snow particles based on either current local temperature, or temperature at cloud top above a grid point. However, this approach did not account for the evolving growth history of the snow field in the different temperature/humidity zones through which it falls. (Hashino and Tripoli, 2007) developed an elegant habit prediction scheme that predicted fundamental habit-related parameters, such as crystal aspect ratio and dendritic arm length, and did so within the context of a bin microphysical scheme. However, such schemes are computationally very expensive and they were only able to apply it to a 2-D model configuration. (Woods et al., 2007) developed a

simpler habit prediction scheme based on the known temperatures and humidities for the growth of various habits. They modified a bulk scheme to track the mass of individual habits by introducing prognostic equations for each new habit's mixing ratio . These mixing ratios were then used to mass-weight the combination of habit-specific parameters to create a single set of adaptable mass-diameter and velocity-diameter relations that governed the behavior of the snow field as a whole. It is this scheme that we have implemented in the WRF model and the testing of this scheme is one of the goals of this study.

Another set of strategies have focused on the effect of riming. One study replaced the individual fall speeds of snow and graupel with one hybrid fall speed based on each category's relative mass (Dudhia et al., 2008). This created a fall speed that was responsive to the amount of riming that had occurred, but could only respond if riming was sufficient to initiate graupel. Another study (Saleeby and Cotton, 2008) took a different approach in which the process of riming itself was modified. While working within a bulk scheme, they calculated collection efficiencies using a binned approach. That is, they divided the assumed size distribution into size bins, calculated collection efficiencies amongst the size bins, and then summed up the resulting collected masses, yielding a more accurate effective collection efficiency value. While this method addresses transfers of mass taking place during the process of riming, it neglected to adjust the fall speeds of snow particles that are affected by the riming. What is lacking in these studies is an attempt to keep track of the portion of snow that has grown by riming, and to allow the degree of riming of snow to feed back into the scheme through altered physical properties of the snow particles, such as mass and fall speeds of particles as a function of their size. This is a major goal of the present research.

1.3 Research Approach

1.3.1 Observational Studies

While other studies have conducted ground-based observations of snow particles, our intent was to create a snow-focused observational data set that was robust in its variety of measured parameters, level of detail, and duration.

At the heart of our approach is the observation of habit type and degree of riming. Our plan involved not only identifying what habits exist, but also their mass-fractional makeup. Our method of observation involved collecting frequent samples of snow particles and directly examining them through a stereoscopic microscope.

In addition to the identification of habit and degree of riming, we measured fall speeds and size distribution of particles using a 2-D video disdrometer. Using such a device gives us the ability to collect data on a much larger number of crystals than the "one crystal at a time" approach that others have used. Further still, we took data on snow depth and snow mass, yielding information on snow density. We also recorded standard meteorological data that included pressure, temperature, relative humidity, and wind.

Lastly, our approach includes taking data for two winters in the Washington Cascades, with the intention of collecting a data set large enough to meaningfully investigate both the relationships among the parameters we measured and the climatological properties of snow in the Cascades.

1.3.2 Microphysics Scheme

Since current bulk microphysics schemes adhere to a single, fixed set of snow particle behaviors, thereby utilizing mass-diameter and velocity-diameter relationships that ignore a particle's specific growth and riming history, our approach is to improve the representation of snow by predicting particle habit and degree of riming, and then dynamically modifying particle behavior accordingly.

First, to make the model sensitive to a particle's shape, we implement within the model a habit prediction scheme developed by Woods et al. (2007), with the specific intention of testing it against the data of several synoptic events obtained during the observational snow study. Then, to make the model sensitive to a particle's riming history, we replace the current prognostic equation for snow mixing ratio with two other prognostic equations: one for the mixing ratio of pristine snow, or the part of snow formed through deposition, and one for the mixing ratio of snow rime mass. This new prognostic riming information will allow the scheme to adjust the properties of snow particles, thereby affecting a myriad of growth processes in the model.

These adjustments will act primarily via changes in the size distribution and fall speed, which in turn change the timing of both growth processes and fallout. Furthermore, an orographic environment is an ideal place to test such a scheme, due to the inherent sensitivity of orographic precipitation to the timescales of particle growth and fallout.

Chapter 2
SNOW PARTICLE OBSERVATIONS

Herein we describe our efforts to gather a data set that meets the goals described in Chapter 1, namely, a long-term observational study of snow particles that contains both highly detailed descriptions of the particle type composition of a representative snow sample at regular observation intervals, coupled with simultaneous measurements of the broader characteristics of the snow, such as fall speeds, precipitation amount, and density of new snow. We also present analyses and distillation of the data that lends insight into the basic behaviors of snowfall in the Cascade Mountains of Washington state. These include an examination of fall speed with respect to varying degree of riming for the same habit type, and the climatological habit and riming composition of snowfall in the Cascades.

2.1 Setup

2.1.1 Measured Parameters

In this study, we looked to measure several important parameters describing the properties of falling and accumulating snow particles:

- Particle Type Identification, Including Habit and Degree of Riming

  The cornerstone of all our measurement goals is the identification of snow particle types with estimates of their mass-fractional percentages. All our efforts are focused on relating the rest of the observed quantities to particle type characteristics and degree of riming. These observations can also be used for evaluation of model-predicted snow crystal habit.

- Liquid Water Equivalent Precipitation

  This measurement is necessary for determining total accumulated mass at each observation time, which can be used to infer accumulated amounts of each particle type.

- Snow Depth

  In combination with the previous parameter, the snow depth allows for the determination of density of new snow accumulation as a function of other quantities (see Casson, 2009).

- Particle Fall Speeds

  This is the key parameter that is expected to vary with habit type and degree of riming. Since it is also an important parameter in microphysical schemes, it is anticipated that fall speed is a key parameter by which a proper treatment of snow particle types in numerical weather prediction (NWP) models will affect their precipitation forecasts.

  Measurement of this parameter for a sufficient number and size range of particles yields a relationship between size and fall speed that can be approximated by a power law. Such power laws are used in bulk microphysical schemes.

- Temperature, Wind Speed and Wind Direction

  These standard meteorological measurements are necessary for assessing changes in synoptic conditions and for relating snow measurements to these standard variables.

2.1.2 Instruments

To accomplish the simultaneous and collocated measurement of the above parameters, we assembled a suite of instruments and equipment that, together with a trailer, were

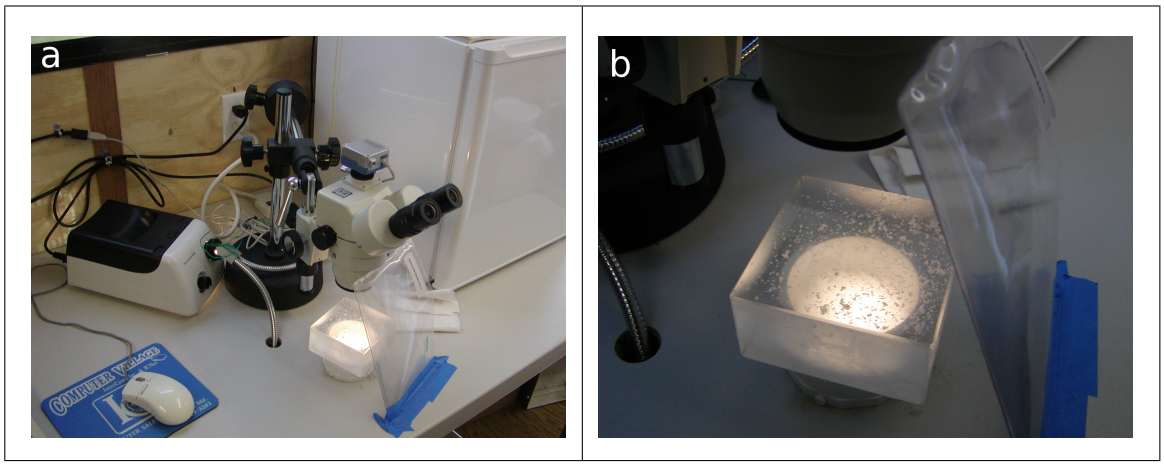

Figure 2.1: Stereoscopic microscope used for habit identification (a) and a closer view of the Plexiglas block used to collect particles (b).

deployed as a mobile snow lab. The trailer transported and housed the equipment, but also doubled as a semi-controlled environment in which to take some of our measurements. In particular, because the observation compartment of the trailer was kept open to the outside air at all times, we had the ability to look at snow crystals under a microscope in a cold but wind-protected, well-lit indoor environment. Neither melting nor sublimation of particles was typically a problem during observation (or even during waiting periods of up to 30 minutes prior to observation, as sometimes occurred), as the observation compartment was usually below freezing and humid.

To observe snow crystals at high power, we utilized a steroscopic microscope with variable magnification in the range of 10x to 40x (see Fig. 2.1(a)). Microscope accessories included compact lighting that, because of its ease of manipulation, was indispensable in aiding identification of the more challenging slides. Three Plexiglas blocks of dimension 10 cm. x 10 cm. x 5 cm. (see Fig. 2.1(b)), were used for catching and observing snow crystals. We used a freezer to pre-chill the Plexiglas blocks and counteract the heat created by the lighting, minimizing the potential for melting.

To measure new snow depth, we fashioned a white, wooden board having dimen-

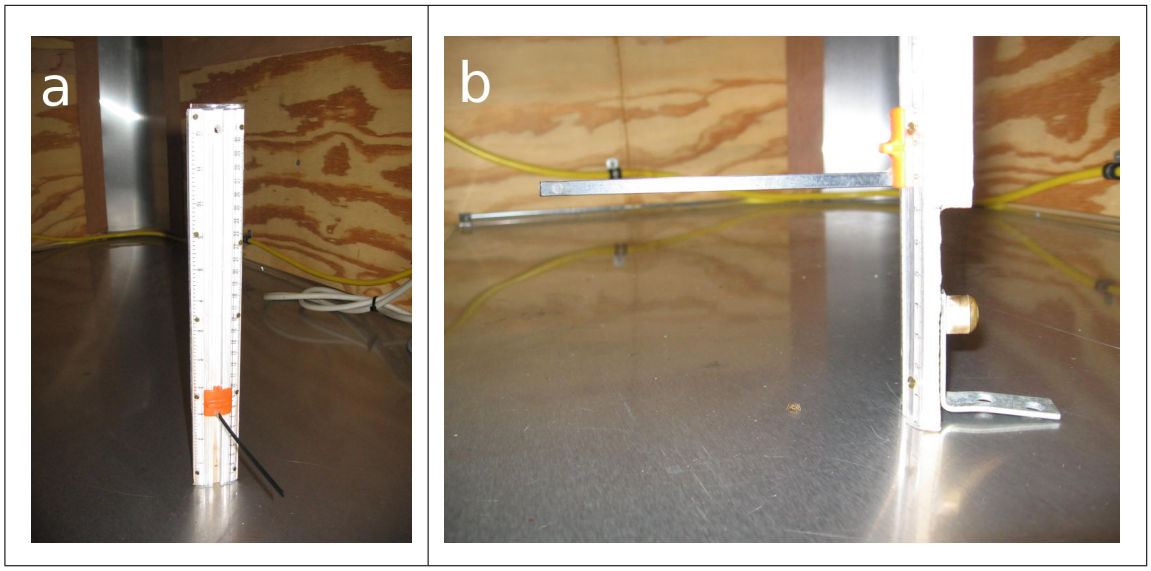

Figure 2.2: Front (a) and side (b) views of the ruler used to make depth measurements.

sions of 40 cm. by 40 cm., and a specially made ruler with a sliding arm that sticks out at an angle of ninety degrees (Figs. 2.2(a) and 2.2(b)) that had a resolution of 1 mm. For measuring the precipitation rate, we constructed a hollow metal cylinder, 90 cm. in diameter and 23 cm. in height, and obtained plastic bags whose mouths fit snugly around the open end of the metal cylinder (see Fig. 2.3(a)). Additionally, we created a ring from a section of brass tubing such that it would rest at the bottom of the metal cylinder, fitting just inside its walls. We weighed the snow bags using a hanging scale with a resolution of 10 grams (which translates to a precision of 0.02 mm of liquid equivalent precipitation), and a range from 0 to 10 kilograms (see Fig. 2.3(b)).

To measure fall speeds and particle sizes we employed a 2-D video disdrometer (see Fig. 2.4). The video disdrometer has two line-scan cameras that provide front and side views of hydrometeors falling through a horizontal opening of 10 cm. square. Photo-detectors were shadowed by the falling hydrometeors, with a pixel resolution

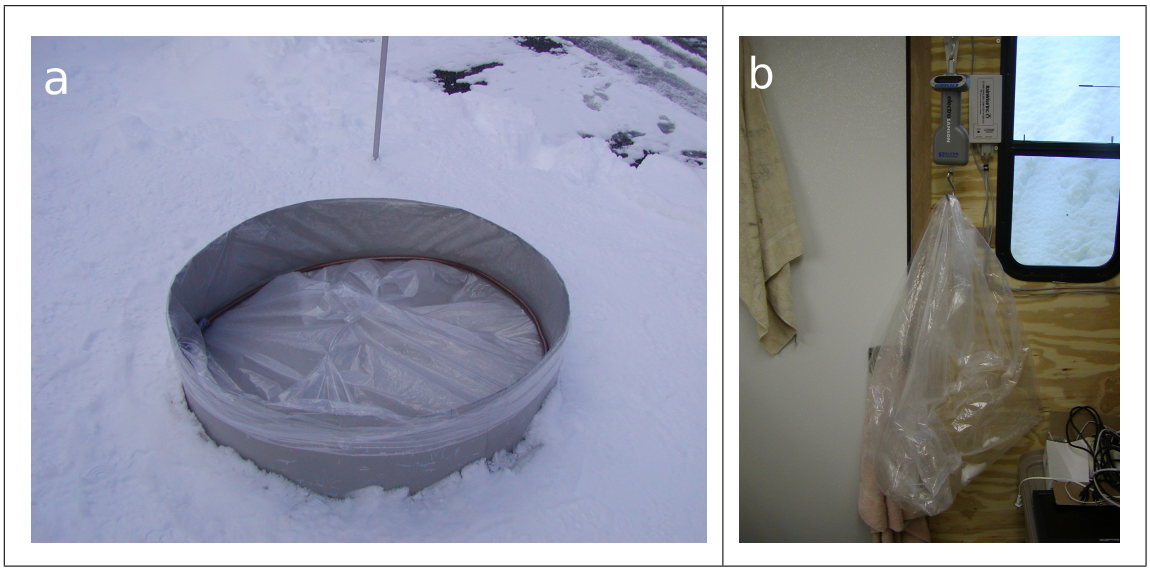

Figure 2.3: Deployed snow bag and snow bag cylinder, used for measuring precipitation rate (a), and the snow bag being weighed (b).

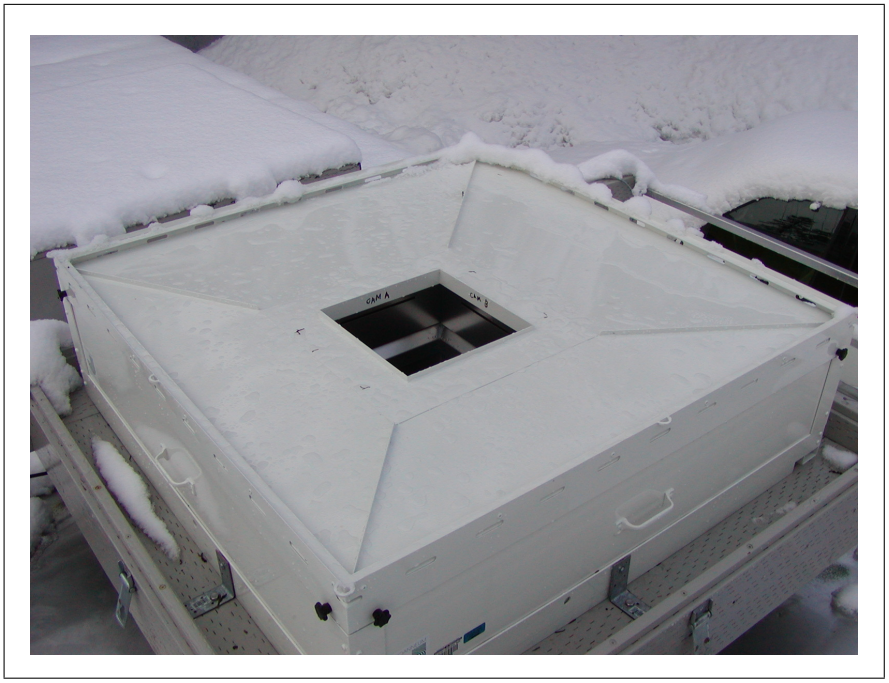

Figure 2.4: 2-D video disdrometer sitting atop the snow lab.

of 150 μm. The camera planes were vertically separated by 7 mm so that particle fall speed could be computed from the time required for the hydrometeors to pass both planes. In addition to providing the fall speed itself, the fall speed information can be combined with the particle count to yield particle size distributions. This instrument, manufactured by Joanneum Research, is described in detail in Kruger and Krajewski (2002).

2.1.3 Site Location

In choosing a location in which to conduct the snow study, it was critical that several criteria were met. First, we sought a region with plentiful snow, to maximize the sampling time, and to observe as full a spectrum of habit types and degrees of riming as possible. The site also needed to be easily accessible in winter conditions, and have affordable housing nearby. Lastly, after experiences from our first year, we came to appreciate the need for a location high enough in elevation to minimize the occurrence of rain, particularly because of the avalanche-related work being done by student Jerry Casson, which focused on the properties of snow after it accumulated on the ground.

For the first winter of our study, we chose a location at Snoqualmie Pass, located at the crest of the Cascades in central Washington state along I-90 at an elevation of 870 m. Meteorologically, the pass receives copious snowfall (approximately 1100 cm. annually), and sees a variety of habit types and riming conditions due to its regular exposure to both maritime and continental airmasses. For such a low elevation, it receives snow more frequently than other similarly elevated locations, since it often experiences an east wind supplying cold air from the interior of Washington during the early to middle parts of synoptic-scale storm passages. Even so, Snoqualmie Pass experienced a higher frequency of rain events than was desirable for the goals of our study, so during the second year, we we relocated to a higher elevation to minimize rain events. We chose Stevens Pass, about 40 km. northeast of Snoqualmie Pass, along state highway 2, at an elevation of 1240 m. Annual snowfall at Stevens Pass

is slightly higher than at Snoqualmie Pass (about 1250 cm.). It is meteorologically similar to Snoqualmie, with the exception of fewer rain events.

In addition to considering where to locate the snow study geographically, we also needed to consider the immediate environment in which the instrument trailer would be placed. Relative to local surroundings, we attempted to place it so that it had a minimum exposure to wind and yet would not be so close to trees that it would be snow snow-shadowed, or receive snow falling out of trees. The Snoqualmie Pass site was surprisingly calm during snow events. At Stevens Pass we did experience more wind, but not frequently enough to have a significant negative impact on the data gathering.

2.1.4 Procedures

While it would have been ideal to make measurements anytime snow fell, resource limitations and logistical considerations prevented this from being the case. Primary among these limitations were the limited number of researchers available to carry out all the observations (2 or 3 for each storm), the large number and complexity of tasks, and the difficulty in predicting snowy periods. In an attempt to get the most from our efforts, we gave preference to situations for which forecasts suggested periods of at least four to six hours of steady snow. These usually involved the passage of fronts, but sometimes this would occur under post-frontal regimes. When a snow event was forecast to last longer than was possible for us to collect data, as sometimes happened when a frontal passage was immediately followed by a very long lasting, orographically forced, post-frontal snow event, we opted to begin collecting data with the arrival of the prefrontal precipitation. This allowed us to cover the entirety of the frontal passage and some of the post-frontal precipitation, depending on how long it took the front to pass. There was a belief that the hours leading up to, and including, the frontal passage likely offered the greatest variety of both observed snow crystal habit and riming. Also, since this period is characterized by changes in

synoptic forcing, it would be the most useful period during which to have data to test a microphysics scheme.

In general, while present at the site we took data as long as precipitation was falling, but if the snow became too intermittent, which compromised the usefulness of our data, we ceased taking data. The most important priority was to continue taking data until the frontal passage was complete. However, the timing of some storms also allowed for the observation of some long periods of post-frontal orographic snowfall, either in addition to or instead of the prefrontal and frontal precipitation.

Setting up the instruments before each event was relatively simple. Both the snow board and metal cylinder were set out in a stable, level place that was far enough from the instrument trailer or any other objects to prevent interference in the collection of snow. The video disdrometer, which was mounted to the top of the instrument trailer, was uncovered and powered on. About once a month, the video disdrometer was calibrated, as recommended by the manufacturer.

When choosing the frequency of manual observations, we settled upon a 15-minute cycle that struck a balance between the need for measurements to be taken as often as possible, and the ability to make those measurements with as much detail and precision as we wanted. This frequency worked well logistically in that, in addition to generally leaving enough time for making measurements, a few extra minutes were often left over in which to address minor emergencies, remedy mistakes, and warm up. As to whether a 15-minute cycle was frequent enough to sample the measured parameters remains an open question. As the project commenced, we soon found that habit type varied greatly between successive measurements, as did the number of habit types appearing simultaneously and the quantity of crystals appearing within a single habit. Since determining these parameters consumed the majority of the measurement cycle, it would be difficult to improve on the frequency of those measurements. Riming, on the other hand, seemed to vary much less. The temporal variability of the snow depth and snow bag measurements was generally moderate, with both long

periods of relatively continuous snowfall, and periods where snowfall clearly varied on a sub-15 minute timescale. Obtaining more frequent snow depth measurements would probably not have helped, because the minimum amount of snow accumulation required for a precise measurement (at least 0.5 cm.) usually took at least 15 minutes to fall.

Of all the measurements, estimating habit mass-percentages and the degree of riming were the most involved. It entailed examining under a stereo microscope precipitation particles collected on a Plexiglas block. With three Plexiglas blocks in rotation, any one block typically had 30 minutes of freezer time before reuse. In all but the absolute warmest of conditions, this proved to be much more than was actually needed. Once a block was removed from the freezer and wiped clean of the tiny crystals that sometimes formed in the freezer or remained from earlier, it was ready for use. At precisely every quarter hour, if there was any precipitation, one team member would take the block outside the trailer, and while standing away from any trees and using their body to shield the block from minor gusts of wind, expose the block to the falling precipitation (see Fig. 2.5(a)). If after approximately one minute it was clear that a proper sample size could not be obtained, the observation was scrapped. Otherwise, once a reasonable amount of precipitation had landed on the block, the block was then taken inside to be studied (see Fig. 2.5(b)). If inspection of the previous sample was complete, then the new slide was immediately analyzed using a microscope, wiped clean when done, and returned to the freezer. If not, the new slide was stored in the freezer until the examination of the previous slide was complete. This infrequent occurrence sometimes happened when a multitude of habit types all appeared on the same slide, when large numbers of crystals belonged to visually similar habit types, or when large numbers of crystals were obscured by riming or other crystals, all of which required a longer and more careful period of examination.

One part of the process that unexpectedly required a bit of practice was deter-

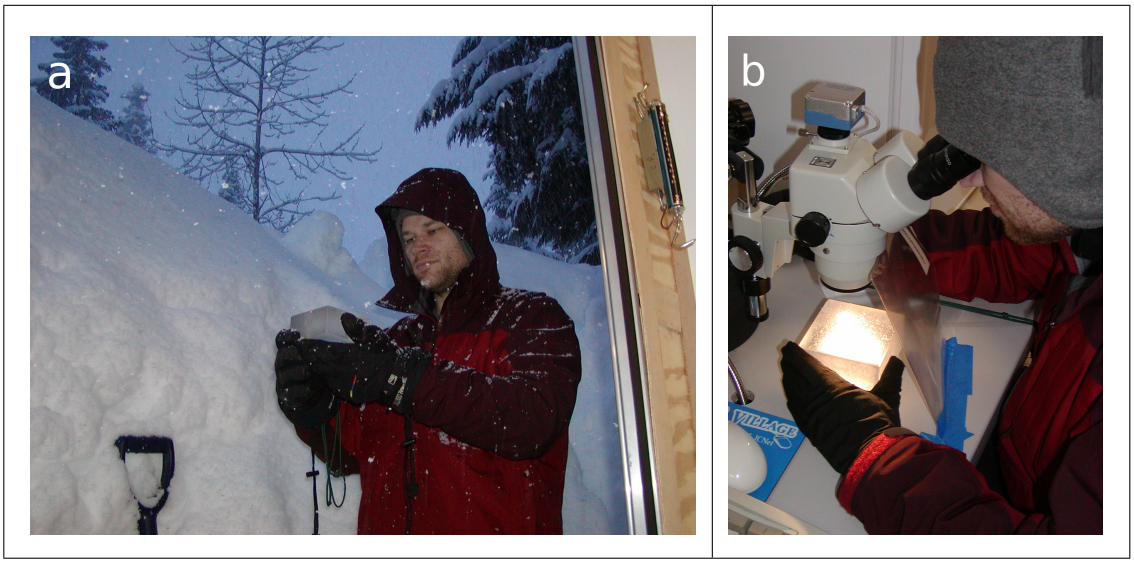

Figure 2.5: Collection of snow particles (a) and particle slide examination (b).

mining how long to keep the block exposed to the precipitation. If the block was exposed for too short a duration, then the sample size would be too small to accurately represent what had actually fallen. If too long, crystals would begin to pile on one another and, especially when aggregates were involved, complicate their identification. Exposing the block for too long also limited the length of time available to complete the examination before the next observation time.

The most challenging part of the process, though, was the examination of the slide. When one of us inspected a slide, we typically began by identifying all the hydrometeors that existed on the slide. Next, we would estimate the percentage of the total mass on the slide belonging to each of the habits just identified. Usually this was done by starting with the those habits that were relatively scarce on the slide and progressing toward those that were more prevalent. Following this, we estimated the degree of riming. This was accomplished by first assessing the general riming level of the overall slide and then assessing any habit's overall riming that differed notably. The degree of riming was judged in terms of the areal coverage of crystal surfaces

rather than by rime mass. Four categories were used, namely unrimed, lightly rimed, moderately rimed, and densely rimed. These riming categories and their definitions are the standard categories and definitions described by Mosimann (1995), except that we replaced their "heavily rimed" category with "graupel-like snow". This term has been used in the literature to refer specifically to particles that are not yet graupel particles, i.e., they still have the appearance of a snow crystal or aggregate, but are too obscured for the habit to be properly identified. After noting the degree of riming, the last step was to describe the degree of melting or sublimation of the crystals if any existed. Note that individual particles (either single crystals or aggregates) were not counted or measured for size. All habit percentages were estimated in terms of percent mass of each type present. Particle counting and sizing was handled by the 2-D video disdrometer.

Making measurements of snow depth was much less complicated. At precisely the same time that one member of the team would sample crystals, a second member would measure the snow depth using the specially made ruler. With the sliding arm on the ruler originally set to be above the snow, the ruler was placed on a cleared section of the board and the arm then adjusted until it just touched the snow (see Figs. 2.6(a) and 2.6(b)). Once the ruler was removed, the position of the arm along the ruler was noted. If the depth of snow became greater than approximately 10 cm., the snowboard was cleared. This was to minimize the possibility of snow depth reductions due to compression and the resultant skewing of density calculations.

As with snow depth, snow bag measurements were made in conjunction with crystal identification observations at every quarter hour. At that time, a "full" snow bag, one that had been collecting precipitation over the preceding measurement cycle, was replaced with an empty one. The process of installing a new empty bag first required that it be weighed, so that later, to get the mass of the precipitation that had been collected over the course of the measurement cycle, the original "dry" mass of the empty bag could be subtracted from the eventual weight of the full bag. To

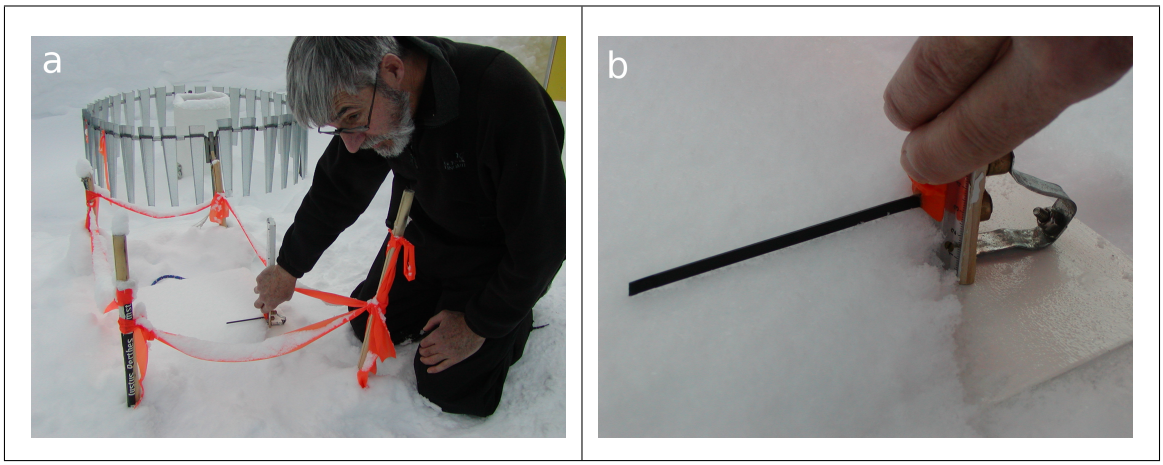

Figure 2.6: Depth measurement location (a) and a close up view of a depth measurement (b).

actually install the snow bag, it was placed inside the metal cylinder, and the mouth of the bag was fit snugly over the top of the cylinder walls. A brass ring whose circumference was just smaller than the metal cylinder's was then placed inside the bag, which functioned to weigh the bag down and keep it in place. The process of retrieving a full snow bag entailed carefully removing the brass ring so that any snow clinging to the ring was returned to the bag. The bag was then removed, again being careful not to lose any of its contents, taken inside, and weighed.

Measurement of fall speeds were largely automated. The video disdrometer measured and logged, on a continuous basis, the speeds of all the particles that fell through its vertically exposed opening. Occasionally, if there had been a particularly heavy snowfall, all snow near the opening was removed to prevent particles from falling in and creating false data points.

2.2 Analysis and Results

2.2.1 Fall Speeds

By associating the particle identification measurements with corresponding video disdrometer data, we hoped to create velocity-diameter relationships for various classes of hydrometeor with specific attention to the affect that degree of riming has for particles of the same habit type. These measurements would go beyond what had been done before in that the video disdrometer captured far more particles than previous "one crystal at a time" methods, allowing for more statistical certainty about the velocity-diameter relationship obtained. At the same time, our extensive and detailed observations allowed us to pick particular times when we were certain that the snow consisted almost entirely of a particular habit type, with a particular degree of riming. To accomplish this, we limited our analysis to those observations in which a single habit type made up at least 90% of the total precipitation mass. Further, to create velocity-diameter relationships that describe narrow degrees of riming, we limited cases to those whose riming was limited to two adjacent categories, such as crystals with moderate to dense riming. In addition we filtered out any cases in which crystals showed any evidence of melting.

To guarantee the particle identification data was representative of the video disdrometer's data, we used video disdrometer data from within a two-minute window only, centered on the time of the particle identification measurement. This was long enough to attain a reasonable sample size, yet short enough to avoid the crystal habit type changing in the meantime.

Before any calculations were made, a minor bit of error checking was done in which a few outlying data points were manually removed. Occasionally, the video disdrometer creates data points that are clearly implausible, which is likely due to the difficulty in correctly matching the two camera images of a particle when two similar particles fall through the instrument nearly simultaneously.

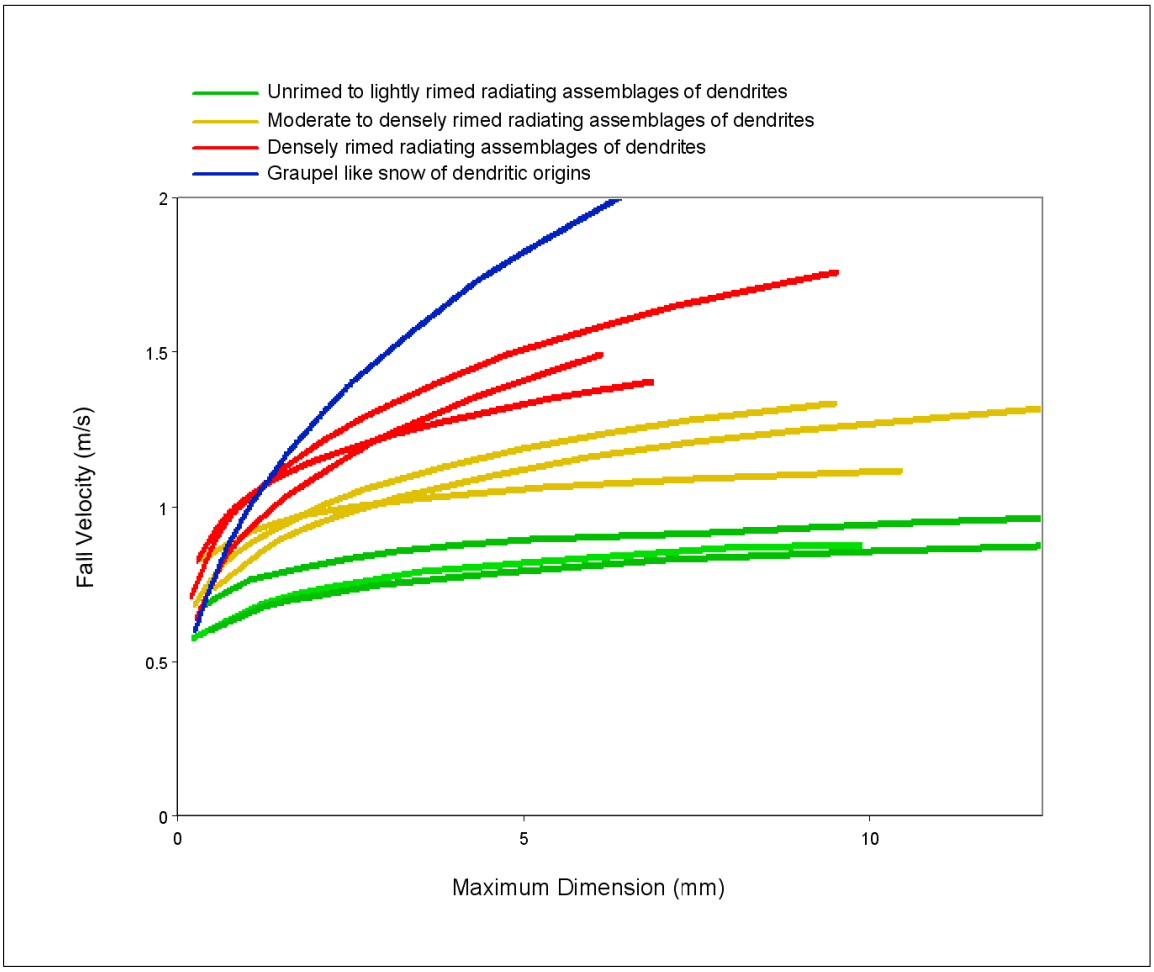

Figure 2.7: Fall speeds of dendrites in various degrees of riming, as observed in the Washington Cascades over the winters of 2006-07 and 2007-08.

Lastly, we fitted the points to a power-law curve of the form $v = a * D^b$, where v is velocity and D is the diameter of the maximum dimension of the crystals. We did this by creating a log-log plot and then using the method of least squares to solve for an appropriate line. Using the slope and y-intercept of this line as our a and b parameters yields an exponential curve that fits the data.

The results are shown in Figs. 2.7, 2.8, and 2.9, which present data for dendrites, needles, and cold-type crystals, respectively. Each curve in these figures represents

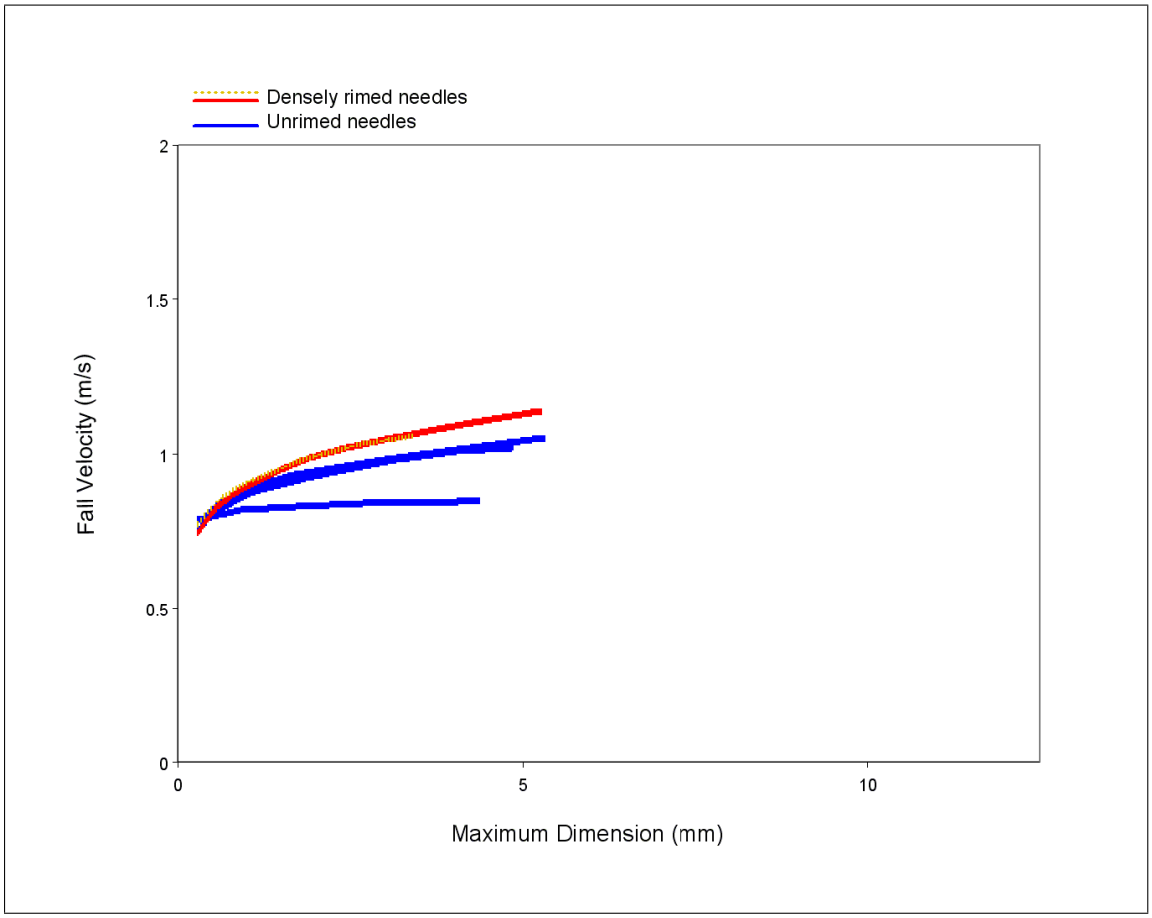

Figure 2.8: Fall speeds of unrimed and densely rimed needles, as observed in the Washington Cascades over the winters of 2006-07 and 2007-08.

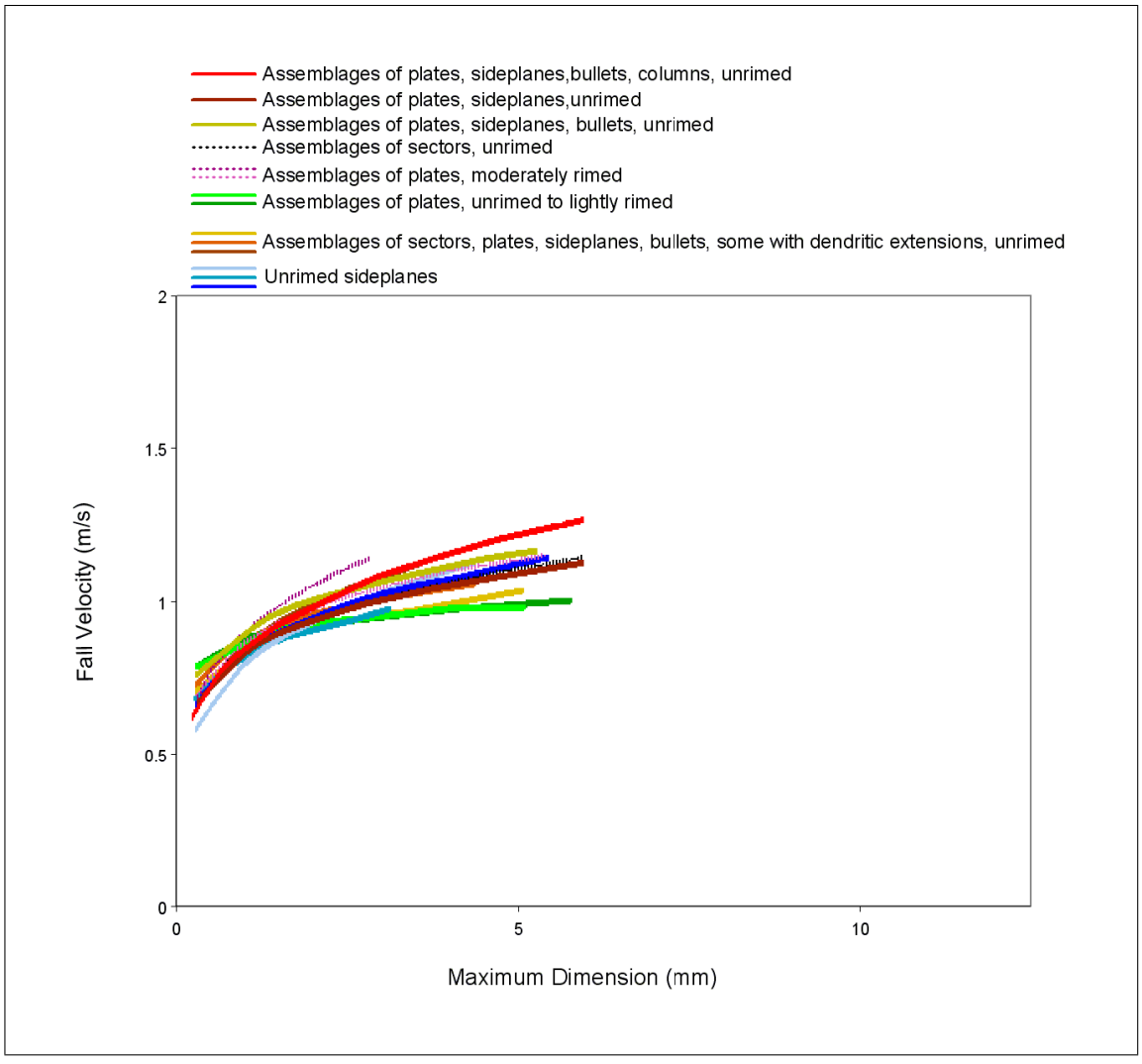

Figure 2.9: Fall speeds of cold-type crystals in various degrees of riming, as observed in the Washington Cascades over the winters of 2006-07 and 2007-08.

the fall speeds associated with an individual 2-minute collection of particle fall speeds of a particular type.

From the graph of dendrite fall speeds (Fig. 2.7) we can see a clear relationship between the degree of riming and the fall speeds of dendrites. In particular, there is a distinct progression from slow-falling unrimed or lightly rimed crystals to more heavily rimed crystals with noticeably greater fall speeds. The fall speeds of needles (Fig. 2.8) appear to be somewhat less affected by increased riming, although far fewer curves are available to identify such a relationship. From Fig. 2.9, we can see that increased riming has little effect on fall speeds of cold-type crystals as well. These results are perhaps unsurprising since the shape of dendrites, which when unrimed typically have many holes and gaps, is considerably more affected by increased riming than that of either needles or cold-type crystals.

Comparing the relative fall speeds of the three categories, needles appear to fall slower than cold-type crystals, while relatively lightly rimed dendrites fall slower than either needles or cold-type crystals. The more heavily rimed dendrites, on the other hand, fall faster than crystals of either of those two categories.

These results stand somewhat in contrast to recent results from a similar study carried out in the Alps. Barthazy and Schefolda (2006) found that among four categories of habits that they considered, which included needles, dendrites, plates, and irregular crystals, the fall speeds of needles increased the most as the degree of riming also increased. More notably, the fall speeds of dendrites seemed almost to not vary at all with degree of riming. When comparing their dendrite velocity-diameter curves to those of this study, the most striking difference is in the unrimed to lightly rimed regime, where their fall speeds appear to be noticeably larger. Within this regime, their sample size was particularly small, consisting of only 27 particles. It is unclear why the two studies reached different conclusions, though our finding of a direct relationship between riming and fall speed for dendritic crystals would seem to agree with intuition.

2.2.2 Particle Type Climatology

As discussed in Chapter 1, a number of studies have documented observed properties of snow particles falling at the ground, some with great attention to detail about particle habits, degree of riming, particle mass, and fall speed. While the results of these studies have been invaluable for setting many key parameters in cloud microphysics schemes, an important piece of information that they have not provided is the long-term, or climatological, documentation of the amount of precipitation reaching the ground in the forms of various frozen particle types. Such information would be highly valuable, because the characteristics of particle types provide useful information on the growth processes that developed those particles. This is true in a qualitative sense for particle habit, which gives an indication of the temperature and humidity conditions at which the particles grew by deposition. It is also true in a more quantitative sense for degree of riming, because the mass of snow grown by riming is, in principle, a quantifiable number, both in nature and in microphysical schemes used to predict precipitation. The fraction of snow grown by riming at a particular location is an important result for these schemes to predict correctly over the course of many storms, because failure to do so is indicative of fundamental flaws in a scheme's representation of snow growth processes. While much effort has been expended to document the microphysical aspects of orographic storm systems in major field studies (e.g., Cascade Project, SCPP, MAP, IMPROVE, IPEX), the basic question of quantifying riming versus depositional growth in the real atmosphere (and properly representing it in models) remains an unsolved issue.

The data gathered in this study provide an opportunity to make a first attempt at such an estimate. While our data set is unique in the number and detail of observations, there are still uncertainties arising from subjective aspects of the data gathering methodology. But the emphasis in our data gathering methodology on both detail of particle observations and extensiveness of sampling, as well as the simultaneous

recording of both precipitation rate and new snow depth, provides a pathway to estimating the long-term percentages of the total masses of different crystal habits, as well as of mass grown by riming versus deposition, for precipitation falling in the Cascade Mountains of Washington state. This information can be used as a test bed for NWP models applied to mid-latitude orographic precipitation.

For any standard, 15-minute observation period, we calculated the amount of collected mass that is attributable to a particular particle type using the equation

$$m_{\text{habit}} \;=\; m_{\text{total}} \left(\frac{1}{2}\, x_{\text{start}} \;+\; \frac{1}{2}\, x_{\text{end}} \right) \tag{2.1}$$

where m_{total} is the total mass collected during a snow bag collection period, and x_{start} and x_{end} are the observed habit mass fractions, as identified under a microscope, at the start and end, respectively, of a snow bag collection period. Occasionally, particularly at times of low rates of precipitation, snow bags were allowed to collect snow for durations longer than the standard 15-minute period. In that case, the amount of mass attributable to a given habit is

$$m_{\text{habit}} \;=\; m_{\text{total}} \left(\frac{\frac{1}{2}\, x_1 \;+\; x_2 \;+\; \cdots \;+\; x_n \;+\; \frac{1}{2}\, x_{n+1}}{n} \right) \tag{2.2}$$

where m_{habit} is the mass attributable to the crystal type, m_{total} is the total mass collected during the same period, x_i is the ith 15-minute measurement of habit mass-fraction associated with a snow bag's measurement period, and n is the number of 15-minute periods over which the snow bag collected mass.

The danger in extending the length of time a snow bag collects data is that doing so implies a constant rate of precipitation, in effect equally weighting each additional habit mass-fraction measurement by the same m_{total}. This becomes problematic, for example, when one or more of the habit mass-fraction measurements are made during a period of particularly intense precipitation and subsequently don't get weighted as heavily as they should. However, the error introduced by this issue is probably

limited, because such periods were usually characterized by low precipitation rate. To further minimize the error caused by such occurrences, our analysis excluded snow bag observations that required more than 1 hour for the snow bag to fill to a measurable amount.

We also filtered out observations in two other instances. First, because the temporal habit variations, even over short periods, were usually quite large, we filtered out any snow bag measurements that were coincident with even one missing habit mass-fraction measurement. Second, when crystals were partially melted or sublimated, identification of crystal type became unreliable, so snow bag measurements during these times were also filtered out.

We applied this methodology to the entire two-winter data set and summed the masses of all the different observed particle types to arrive at a list of the total mass percentages of all these types that fell at our two locations during the two winters (although not all times during all storms were observed, as discussed earlier in this chapter).

This full list is not shown here, because it includes over 100 different particle types, and it is somewhat difficult to interpret; no single type comprises more than a few percent of the total (with the exceptions of graupel and graupel-like snow), so the relative occurrence of basic habit types does not emerge from this comprehensive list. Therefore, we chose to create a limited number of categories of hydrometeors for characterizing the mass percentages that fell during the study. The categorization took into consideration different attributes of the habit types, including similarity of shape, and similarity of temperature and humidity conditions for growth. The six categories are:

1. Dendritic: any branched crystal type of the dendritic variety, including stellars, that grow at water saturation at approximately -13 to $-17\,^{\circ}\mathrm{C}$.

2. Cold-type: a class of crystals that grow from -20 to $-30\,^{\circ}\mathrm{C}$, including sideplanes,

assemblages of plates, and assemblages of sectors.

3. Needles: long, pointed crystals that grow at water saturation at temperatures between -5 and $-10\,^{\circ}$C.

4. Columns: column-shaped crystals of hexagonal cross section, that grow under a variety of conditions.

5. Plate-like: any crystals of flat, hexagonal plate shape, including plates, broad-branched crystals, and sectors, that grow under a variety of conditions.

6. Bullets: columnar crystals with tapered ends that grow at temperatures colder than $-30\,^{\circ}$C, initially in "rosettes", although individual bullets often break off to produce individual bullets.

One issue that had to be resolved was the categorization of occasional multi-habit particles, in which a particle's different habits fall into two or more different general categories (e.g., columns capped by stellars, plates with dendritic extensions, etc.). We partitioned the masses of such particles using simple fixed percentages, based on the observers' experience of examining hundreds of such particles, and estimating the average mass percentage of a typical particle that should be assigned to each category. For example, bullets capped by stellars were partitioned 70% to "Bullets" and 30% to "Dendritic". In reality, these multi-habit particles comprised a small percentage of the total particles observed, so the error introduced by this partitioning is expected to be small.

The results of the climatology, after grouping the habits into the six categories, are shown in Table 2.1. Before addressing the habit amounts, a few non-habit categories should be described. The most prominent result in the table is the prominence of graupel-like snow (21% of total mass), indicating the climatological importance of riming to precipitation growth at this location. True graupel comprises a far

Hydrometeor	Portion of Total Mass
Graupel-like Snow	21%
Graupel	6%
Bullets	4%
Cold-Type	18%
Dendrites	25%
Plate-like	6%
Columns	6%
Needles	8%
Frozen Drops	4%
Unknown	<1%

Table 2.1: Each hydrometeor type's portion of the total particle mass observed over the winters of 2006-07 and 2007-08.

smaller fraction (6%), indicating the less frequent occurrence of sufficiently intense convectively-generated vertical motions required to produce the copious liquid water that leads to the formation of true graupel particles. Frozen drops (4%) represent a small but non-negligible contribution to the total precipitation. The final category in Table 2.1 is "Unknown" which refers to snow particles that did not conform to any known habit shape. This category comprised essentially a negligible percentage of mass, reinforcing the point made in Stoelinga et al. (2007) that when particles are examined in sufficient detail with a stereo microscope, nearly all are identifiable according to standard habit particle classification schemes such as (Magono and Lee, 1966), as opposed to the conclusions of studies based on Formvar impressions (Barthazy and Schefolda, 2006), 2-D shadow photography (Rauber, 1987), or 2-D aircraft imagery (Korolev et al., 1999, 2000; Korolev and Isaac, 2003), which tended to find

that most particles fall into an "irregular" category.

Crystal Habit	Habit Mass Fraction	Pristine Portion of All Habit Mass	Rime Portion of All Habit Mass	Habit Rime Mass Fraction
Bullets	6%	6%	<1%	6%
Cold-Type	27%	25%	2%	7%
Dendrites	39%	32%	7%	19%
Plate-like	7%	6%	<1%	12%
Columns	9%	7%	2%	23%
Needles	12%	10%	3%	22%
All Habits	100%	85%	15%	15%

Table 2.2: Each crystal habit's portion of the total mass of all habits observed over the winters of 2006-07 and 2007-08, both as a total and broken into its pristine and rime constituent parts. Also expressed is the rime percentage of each habit's total mass.

About 68% of the total mass is associated with particles that are sufficiently unrimed such that their habit could be determined. If the percentages are re-normalized by the total of only the habit-recognizable snow particles, the percentages become those listed in the first column of Table 2.2. It can be seen that dendritic types comprise nearly 40% of the total mass of snow that reaches the surface. Considering that dendrites grow only at water saturation, and in a fairly narrow temperature range (approximately -13 to $-17\,^{\circ}$C), it may at first seem unlikely that dendrites would comprise such a large portion of the mass. However, there are several factors that increase likelihood of dendritic snow growth within storms. First, the temperature range at which dendrites grow corresponds to the temperature range of highest absolute excess of water vapor above ice saturation at water-saturated conditions. This means that for a given ascent rate, this is the temperature at which the maximum

forcing for depositional growth is possible before the achievement of water saturation limits further supersaturation with respect to ice. Second, the typical height of the $-15\,^{\circ}$C level (the midpoint of the dendritic range) is at 3 to 4 km. altitude in Pacific Northwest winter storms, which also corresponds to the typical level of maximum ascent in such storms. Third, while moisture supply generally maximizes in the lowest atmospheric levels, and active ice nucleus concentrations are most plentiful at the coldest temperatures, the dendritic growth zone may well represent an optimal overlap of both sufficient moisture supply and sufficient ice particle concentrations to take up the large moisture supply. Finally, dendritic crystal structure is well suited to maximize depositional growth. The lengthy branches extend away from the center of the growing crystal and into the environment, where humidity is higher, and the large surface area of the branched structure allows the crystals to quickly dissipate latent heat produced through deposition, and maintain large supersaturation with respect to ice. In a study of Wyoming snow storms, Auer and White (1982) found that a disproportionately large fraction of heavy snow storms were comprised largely of dendritic crystals, and that in these storms, the level of maximum ascent corresponded with the dendritic growth temperature range.

The second most prevalent habit category is the cold-type category. These habit types are of interest because they grow at temperatures in the atmosphere (-20 to $-30\,^{\circ}$C) that range in altitude from 4.0 to 5.5 km., where mid-tropospheric baroclinically forced lifting 100 km or more upstream of the barrier is more likely the cause of their formation than lower-tropospheric orographic lifting over the windward slopes. Thus, to first order, their mass percentage is a quantitative indicator of the importance of large-scale baroclinically driven ascent, compared to orographically driven ascent, for precipitation that falls over the mountains.

Needles are not uncommon (12% of habit-identifiable mass), which is not surprising considering the strong orographic forcing that often occurs within the lower troposphere at relatively warm temperatures, particularly in post-frontal orographic

environments where the entire cloud is sometimes confined to temperatures warmer than $-10\,^{\circ}\mathrm{C}$. Interestingly, the two habit types that are usually thought of as the simplest and most canonical structures, plate-like and columnar, actually comprise, with the exception of the "Bullets" category, the smallest mass fractions of any of the categories considered here.

As suggested earlier, another important problem is quantifying the contribution of riming to the total mass of precipitation reaching the ground. To address this problem, we require a means for calculating the rime mass fraction (RMF) for each observed particle type. This quantity was not measured directly, but can be inferred from the available information, subject to a few assumptions.

Riming Description	Degree of Riming
Unrimed	0
Unrimed to Lightly Rimed	5
Lightly Rimed	10
Lightly Rimed to Moderately Rimed	30
Moderately Rimed	50
Moderately Rimed to Densely Rimed	75
Densely Rimed	100

Table 2.3: Riming descriptions and their equivalent degree of riming.

The first step is mapping each qualitative riming category to a numerical value, referred to here as "degree of riming" (DOR). We define DOR as the amount of rime mass on a crystal, expressed as a percentage of the rime mass on a "densely rimed" crystal of the same habit type. The assumed mapping of riming category to DOR is shown in Table 2.3. The scaling was derived from the observers' best estimate of the typical number of droplets per unit area on a crystal of a given riming category

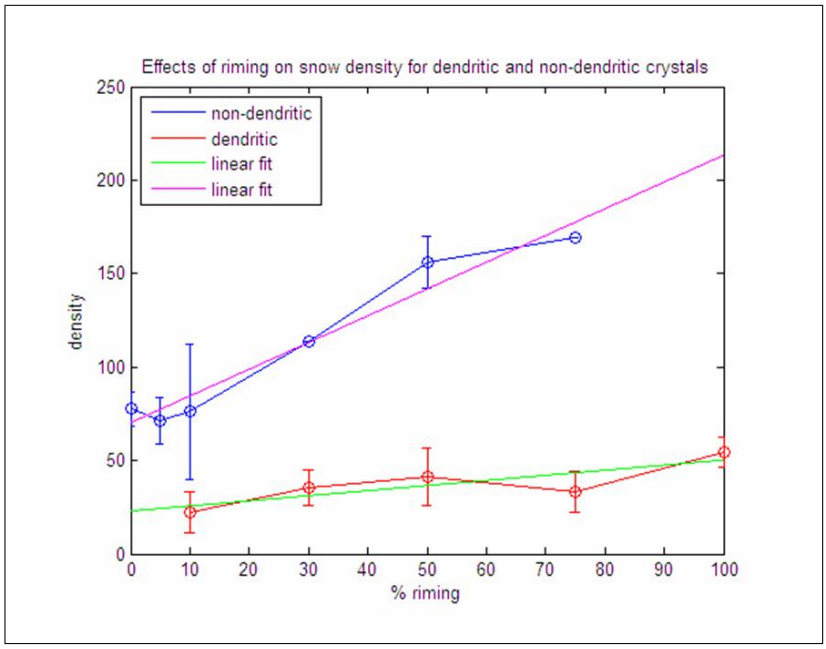

Figure 2.10: Density of dendritic and non-dendritic crystals in the Washington Cascades over the winters of 2006-07 and 2007-08, as a function of their degree of riming.

compared to the number per unit area on a densely rimed crystal of the same habit type, based on their experience looking at many thousands of rimed crystals.

The next step is to calibrate DOR so that it can be used to quantify particle RMF. We did not measure particle riming mass fractions directly. However, we did measure depth and mass of new snow accumulations on the ground, from which we could quantify bulk densities of accumulated snow. Master's research from Casson (2009) included an analysis of how the density of accumulated new snow varies with DOR (defined as above and scaled as in Table 2.3) for two classes of particle types, dendritic and non-dendritic (see Casson, 2009, for details of his analysis). The results of that analysis are shown here in Fig. 2.10, and the least-squares linear fits are:

$$\text{Dendritic}: \quad \text{density} = (0.27 * DOR + 23.0)\,\frac{kg}{m^3} \tag{2.3}$$

$$\text{Non}-\text{dendritic}: \quad \text{density} = (1.43 * DOR + 70.2)\,\frac{kg}{m^3} \tag{2.4}$$

We approximate the RMF of the accumulated snow as

$$\text{RMF} = \frac{\rho_{\text{rimed}} - \rho_{\text{unrimed}}}{\rho_{\text{rimed}}} \tag{2.5}$$

where ρ_{rimed} is the density value on one of the fitted lines in Fig. 2.10 for a given DOR, and $\rho_{unrimed}$ is the density value on one of the fitted lines at zero DOR. Combining (2.3), (2.4), and (2.5) yields the following expressions for RMF:

$$\text{Dendritic}: \quad \text{RMF} = \frac{DOR}{DOR + 85.2} \tag{2.6}$$

$$\text{Non}-\text{dendritic}: \quad \text{RMF} = \frac{DOR}{DOR + 49.1} \tag{2.7}$$

One important assumption has to be made in order to accept (2.5) as a valid estimate of the RMF. In principle, the expression for RMF in (2.5) should be in terms of mass, but instead it is expressed in terms of our measured quantity of density (mass per unit volume). Therefore, in order for (2.5) to be approximately valid, the difference in masses of a given accumulation of rimed snow particles and a hypothetical accumulation of identical but unrimed snow particles must be much larger than the difference in volumes of the same two accumulations. It is postulated here that this is a good assumption since, in the experience of the observers, particles usually exhibited a complex 3-D structure either due to their habit type (e.g., radiating assemblages of dendrites or plates), or their tendency to combine into aggregates, or both. Rime mass tended to accumulate throughout the particle on both its interior and exterior surfaces, so that the particle's volume changes proportionally much less than does its mass when it is rimed. This is true until the point that the particle's degree of riming

exceeds that of "graupel-like snow", after which additional riming accumulates only on the outside of the particle, and particle mass and volume thus increase at a similar rate.

Hydrometeor	Rime Mass Fraction
Snow	15%
Graupel-like Snow	75%
Graupel	100%
Total	34%

Table 2.4: Percentage of each hydrometeor's total mass that was made up of rime, as observed over the winters of 2006-07 and 2007-08. The total represents a mass-weighted average of the three categories.

We applied (2.6) to all the mass that fell in the the dendritic type category, and (2.7) to the other five habit categories. The results are shown in columns 3 through 5 of Table 2.2. Column 3 gives the depositionally grown, or "pristine" mass, associated with a particular habit category, as a percent of all the mass (rime and pristine) in all identifiable habits. Column 4 gives the riming mass associated with each habit category, again as a percent of the total mass of all identifiable habits. The bottom row gives the values for all habits. Thus, the total mass due to riming for all particles whose habit type is identifiable is 15%. This number may seem small, but recall that it includes unrimed and lightly rimed snow, as well as moderately and densely rimed. Also, this number excludes graupel-like snow and graupel, which contain significantly more rime mass (discussed next). Because the RMF for particles of identifiable habit is not that large, the relative prominences of the different habit categories are qualitatively the same when ascertained from pristine mass only (column 3 of Table 2.2) as from total mass (column 2, discussed previously).

The habit category in Table 2.2, column 4, that is associated with the greatest

contribution to total rime mass is dendritic, both because it is the most prevalent habit type, and it is, on average, composed of a greater percentage of rime than several other habit types (i.e., it has a large RMF). This latter quantity, the RMF for each habit category, is listed in column 5. An examination of RMF for the different habit categories reveals a distinct pattern. A habit's RMF generally increases as the temperature at which the habit grows gets warmer. This makes sense, in that at warmer temperatures, vapor is more plentiful, so that if water saturation is achieved, more supercooled cloud liquid water is likely to be produced. Therefore, crystals that are present at warmer temperatures are likely to encounter more liquid water and be more heavily rimed. The fact that crystals that grow at colder temperatures are much less rimed also suggests that the scenario of crystals growing at high altitudes and then falling through low-level clouds rich in liquid water is not common. This indicates that strong lifting aloft (to produce the crystals) is typically not accompanied by strong lifting at low levels (to rime them). This result is in general keeping with what previous investigators have described to be the typical evolution of precipitation production as synoptic systems move across the Cascade Mountains (Hobbs, 1975).

The mass percentages of graupel-like snow and graupel (Table 2.1) indicate that much of the rime mass in Cascade Mountain precipitation comes in the form of habit-ambiguous forms, which was not accounted for in the numbers in Table 2.2. However, the same procedure can be applied to these categories as was applied to the habit-identifiable categories, to obtain their RMF. In the case of graupel-like snow, we used (2.5) to obtain RMF, substituting our observed two-season average density of accumulated graupel-like snow (91.7 $\frac{\text{kg}}{\text{m}^3}$) for ρ_{rimed}, and the linear fit for density of dendrites at DOR = 0 (Fig. 2.10) for ρ_{unrimed}. We used the dendritic line because circumstantial evidence usually suggested that the graupel-like snow particles were of dendritic origin (e.g., other simultaneously falling but less rimed particles were typically dendritic, or an occasional dendritic branch could be seen protruding from the particle). These assumptions yielded an average RMF for graupel-like snow of

75%. For true graupel particles, we assumed a RMF of 100%. The results of total RMF for habit-identifiable snow, graupel-like snow, and graupel, are shown in Table 2.4, along with a mass-weighted total. Thus, for all frozen precipitation observed during the entire two seasons, approximately two thirds is estimated to have come from depositional growth, and approximately one third from riming growth.

Obviously this number would be far more valuable if accompanied by some estimate of its uncertainty. While we did not perform a rigorous quantitative uncertainty analysis, we reviewed the derivation of this number, starting with the subjective observation technique, and the assumptions made in the derivation, and we estimate that the true number for total riming mass fraction is probably no lower than 25%, and probably no higher than 45%.

Chapter 3

RIMING AND HABIT PREDICTION

Based on the work of previous observational studies as well as our own observational climatology described in Chapter 2, it is clear that there are significant differences in snow particles that are identifiable in observations, and that probably effect the growth of precipitation, particularly in orographic regimes. As mentioned in the introduction, most bulk microphysical schemes that are used in numerical weather prediction models treat snow in a highly simplistic way, often as spheres of constant density regardless of the history of growth of snow particles due to deposition and riming. Such schemes may well be failing to capture important particle type-related effects on precipitation growth.

In the present study, two separate but related efforts were carried out in an attempt to improve upon this situation. The first was to port a snow habit prediction scheme to the WRF model's Thompson microphysical scheme, and to test that scheme by comparing its results with observations. The snow habit prediction scheme was developed by Woods et al. (2007), and was originally implemented in the version of the Thompson scheme within the Penn State University / National Center for Atmospheric Research Mesoscale Model Version 5 (MM5). The second effort was to add a new methodology to the WRF Thompson scheme to separately predict the riming and depositionally grown mass of snow, and to modify snow characteristics based on those predictions. This new riming prediction scheme is described and its behavior analyzed in a single case study.

3.1 Mesoscale Model Used

All numerical simulations were performed using version 2.2.1 of the Weather Research and Forecast Model (WRF) utilizing the Advanced Research WRF (ARW) dynamic core, (Skamarock et al., 2005). For these simulations we also chose both the CAM longwave and shortwave radiation scheme (Collins et al., 2004), the the Yonsei University (YSU) boundary layer scheme (Hong and Pan, 1996; Noh et al., 2003; Hong et al., 2006), and the Kain-Fritsch cumulus parameterization scheme (Kain, 2004). The WRF was configured to make use of both nudging and positive advection.

For the microphysics scheme, we chose the Thompson scheme (Thompson et al., 2004, 2008), a five-species, single-moment (double-moment for cloud ice), bulk microphysical scheme. Its snow size distribution consists of a combined exponential/gamma distribution that reproduces the frequently observed "shoulder-shaped" size distribution for snow particles seen in aircraft observations (Field et al., 2005). One reason for choosing this particular microphysics scheme was our research group's considerable experience in using, and familiarity with the details of, this scheme.

Our high-resolution runs made use of four recursively nested domains with resolutions of 36 km., 12 km., 4 km., and 1.33 km., respectively, while our low-resolution runs made use of the 36 km. and 12 km. domains only. The domains are roughly centered on the Cascades of central Washington, except that they extend further out along their western edge to cover the region of prevailing upstream flow. These domains were configured for 38 vertical model eta levels, and the terrain of the highest-resolution domain was smoothed with eight passes to prevent problems sometimes common to sharp terrain.

3.2 Habit Prediction

An early part of this master's research involved the porting of the Woods et al. (2007) habit prediction method from the Thompson scheme in the MM5 model to

the Thompson scheme in the WRF model. This porting was completed successfully, allowing for the testing of the scheme within a more state-of-the-art mesoscale model. The discussion of the habit prediction work will be kept brief for two reasons. First, the current work's author was not involved in the development of that scheme; second, the results were not particularly encouraging. Although specific suggestions will be presented as to how the performance of the habit prediction scheme might be improved, it was decided that the focus of the current work should be on the development of the riming prediction scheme. Below is a synopsis of the habit prediction implementation and testing.

The goal of habit prediction is to model the physical characteristics of snow more realistically, choosing a set of behaviors that are responsive to current environmental conditions and to the snow field's accumulated history. Since particles that formed in differing regions of temperature and humidity have unique physical properties, the mass accumulated in a particular habit's growth region can be individually tracked by means of a new equation predicting the habit's mixing ratio. From these mixing ratios, a single set of mass-diameter and velocity-diameter relations can be obtained by mass-weighting the habit-specific behavioral parameters. These habit-adjusted parameters then govern the snow field as a whole.

To evaluate the habit prediction scheme, we compared its output with observations we made over the course of our two seasons in the field. We chose three observed storms from Snoqualmie Pass and three from Stevens Pass, based on several criteria. Minimally, we looked for cases that had several hours of uninterrupted data taking, very minimal rain or sleet, periods of riming, limited numbers of simultaneously observed crystal types, and a large scale shift in the crystal type regime. Further, any case having other desirable characteristics was given extra consideration. These characteristics included generally having only one predominant crystal type at a time (i.e. making up 80% or 90% of the total mass), minimal short-term crystal type variation, a variety of riming, and the existence of dendrites.

We then compiled for the duration of the event the observations of crystal habit, habit mass fraction, and precipitation rate. We used the method discussed previously in Chapter 2 to calculate the amount of mass that each habit contributed to the total measured precipitation over each 15-minute interval, creating plots of the time-series, converted to units of hourly rate. Then, using the snow study's location at the time of each synoptic event, we made equivalent time-series plots of the model's forecast of the contribution that each habit made to that precipitation rate at the ground.

Comparing the time-series graphs, we discovered that while dendrites appeared quite often in observations, the model seemed to have tremendous difficulty reproducing them, succeeding only rarely and in small amounts. While the model also had some difficulty producing needles, the deficiency was less pronounced than with dendrites. Within the habit prediction scheme, these two habits are the only categories represented exclusively by growth regions above water saturation. This suggests the model is either having difficulty achieving water saturation or having difficulty producing crystals in the dendritic and needle temperature ranges. Correspondingly, the model also grossly overproduced sectors and columns. Though these two categories include growth regions below water saturation for the temperatures at which dendrites and needles form, respectively, they also include other growth regions. Therefore their overproduction doesn't prove that the fault for the lack of dendrites and needles lies within the model's inability to achieve water saturation, but it is consistent with that hypothesis. Further, it seems unlikely that growth would occur in great measure in all the temperature ranges surrounding the growth region of needles and dendrites while somehow failing to produce those crystals. Therefore, our over all conclusion with regard to the habit-prediction approach is that it failed to produce sufficient snow mass in habits that require water saturation for growth because water saturation was not achieved in the model as prevalently as in the real atmosphere. The reasons for this failure must be tied to the basic processes that either supply water vapor for hydrometeor growth (vertical air motions) or remove that water vapor prior to

achievement of water saturation (depositional growth). In other words, the failure is likely due to either an inability to produce the true magnitude of vertical velocity that occurred in nature, or to an overactive depositional growth process at subsaturation with respect to water that prevented water saturation from being achieved. If a lack of upward motion is the cause, an immediate suspicion is cast on the model resolution, since lower resolution generally yields weaker upward motion, especially over complex terrain. However, we did run the model at different resolutions (12 km. and 1.33 km), and this did not seem to alter the problem. If overactive depositional growth at sub-water saturation is the cause, additional work might focus on adjustments to the capacitance for depositional growth, which itself is habit-dependent, and may well be over simplified and too large in the bulk scheme. Finally, another option to "force" the scheme to behave properly would be to lower the threshold relative humidity at which water saturated habits develop until the model matches observed quantities of these habits. However, such an arbitrary adjustment would likely have to be tuned for each location, synoptic situation, etc.

One caveat about the comparisons made here between the model and observations is that, because of the highly variable topography, observations at a single point may capture highly localized effects caused by the topography that aren't experienced even a short distance away, and the model grid may not adequately represent highly localized phenomenon. Even assuming the model was able to correctly mimic what actually occurred at a grid point, because of the likelihood that the location of interest does not coincide exactly with the one of those grid points, the model may be forced to interpolate values from several points experiencing dissimilar phenomenon.

3.3 Riming Prediction

3.3.1 Description of Scheme

In developing the riming prediction scheme, we chose to build upon the habit prediction scheme discussed above, but in such a way that habit prediction could be turned on or off independent of riming prediction. For simplicity's sake, what follows is a description only of the riming prediction methodology, independent of the prediction of separate habits.

Fundamental to the design of the riming prediction scheme is the role of two competing growth processes: deposition and riming. Depending on the relative strength of these two processes, particles can take on a final form that ranges from those produced entirely by deposition, as with unrimed crystals, or those that are produced almost entirely by rime, as with graupel. In what follows, snow mass that derives from depositional growth is referred to as "pristine", whereas mass that is formed by riming is called "rime".

As the name implies, the goal of the riming prediction scheme is to predict at a given location the amount of rime mass that should exist at any moment in time. Since the unmodified microphysics scheme includes only a single prognostic equation representing all snow mass, we replaced it with two prognostic equations, one for the pristine mass, and one for the rime mass, as shown in simplified form below.

$$\frac{dq_s}{dt} = \text{deposition} + \text{autoconversion} + \text{riming} + \text{other} \tag{3.1}$$

$$\frac{dq_{s,prist}}{dt} = \text{deposition} + \text{autoconversion} + f_{prist} \times \text{other} \tag{3.2}$$

$$\frac{dq_{s,rime}}{dt} = \text{riming} + f_{rime} \times \text{other} \tag{3.3}$$

$$f_{prist} = \frac{q_{s,prist}}{q_s}; \quad f_{rime} = \frac{q_{s,rime}}{q_s} \tag{3.4}$$

In the above, qs is the total snow mixing ratio, and (3.1) is the original prognostic

equation for snow. qs_{prist} is the mixing ratio of pristine mass only, and qs_{rime} is the mixing ratio of rime mass of snow only. Equations (3.2) and (3.3) are the separate prognostic equations for these snow partitions. Note that at any given time,

$$qs = qs_{prist} + qs_{rime}$$

and similarly the two component equations exactly sum to the original equation. The two component equations differ in that all depositional growth terms supply mass only to qs_{prist}, and all riming-related terms supply mass only to qs_{rime}. The derivatives on the left-hand side are Lagrangian, indicating that the snow partitions are separately advected in three dimensions. All microphysical production terms for snow that are not specifically related to depositional growth or riming (the "other" in the equations) are assigned to the two snow partitions in proportion to their fraction of the total snow mass at a grid point, as expressed with the mass fractions designated f_{prist} and f_{rime}.

Among the "deposition" terms are the depositional growth of snow, autoconversion of cloud ice to snow, and collection of cloud ice by snow. The latter two processes are considered deposition because cloud ice typically grows from deposition only. Among the "riming" terms are collection of cloud water by snow, collection of supercooled rain water by snow, and loss of rime due to rime-splinter ice multiplication. The "other" terms include sublimation, loss due to collection by warm rain, and melting.

This partitioning of the snow field allows for the separate quantification of snow mass grown by the distinct processes of deposition and riming, which is interesting in and of itself. However, riming prediction only becomes useful to the forecast when it is allowed to affect the physical properties and behavior of snow particles. One property that must be considered is a particle's size. Prior to formation of graupel, we assume that riming increases a particle's mass without affecting its size. The reason for making this assumption, also described in Chapter 2, is based on our observations that as rime collects on a crystal, it tends to fill in the gaps without

increasing its diameter, until the particle's degree of riming exceeds that of graupel-like snow (GLS). This is an important assumption to make because it allows us to define the size distribution as that which would occur if the snow consisted only of the current pristine mass alone. The consequence of this assumption is that a rimed population of particles are generally smaller than an unrimed populations consisting of the same mass, which makes physical sense.

Of equal importance to the size distribution is the way that riming prediction is allowed to affect the mass-diameter and velocity-diameter relationships for snow. These relationships appear throughout the bulk microphysical scheme and effect virtually every production term for snow. The two relationships are usually described by the power law equations

$$m = a_m D^{b_m} \tag{3.5}$$

and

$$v = a_v D^{b_v} \tag{3.6}$$

respectively, where m is the mass of a particle, v is the fall speed of a particle, D is the diameter of the particle, and a_m, b_m, a_v, and b_v are all empirically derived values. In habit prediction, each habit is associated with a different set of a and b constants. However, here we consider only a single set of constants for pristine snow, a_{mp}, b_{mp}, a_{vp}, and b_{vp}, which are empirically derived values from measurements of one habit type or an average of habit types. We seek adjusted constants a_m, b_m, a_v, and b_v, to be used when a fraction of the snow mass is rime.

To determine the adjusted mass constants, we first appeal to Locatelli and Hobbs (1974), who found that, for a given habit type, the exponent in the mass-diameter relationship b_m changed little for different degrees of riming. Most of the change in mass was expressed as changes in the coefficient a_m. This effectively means that for a given habit and degree of riming, the ratio of the mass of a rimed particle to an unrimed one is independent of size. Therefore, we made the simplifying assumption

that the riming adjustment to the mass power law should only be in the coefficient, not in the exponent (i.e., $b_m = b_{mp}$). Next, we evaluate the integral of snow particle mass across the entire size distribution to yield the mass concentration:

$$\begin{aligned} m &= \int_0^\infty a_m D^{b_m} \; N(D) \; dD && (3.7) \\ &= a_m \int_0^\infty D^{b_m} \; N(D) \; dD && (3.8) \\ &= a_m M(b_m) && (3.9) \\ \therefore \quad M(b_m) &= \frac{a_m}{m} && (3.10) \end{aligned}$$

where m is the snow mass concentration, $N(D)$ is the size distribution, and $M(b_m)$ is the b_mth moment of the total snow population's size distribution. For a hypothetical snow population that is completely unrimed but contains the same amount of pristine mass as the rimed population,

$$M(b_{mp}) = \frac{a_{mp}}{m_p} \tag{3.11}$$

where $M(b_{mp})$ is the b_{mp}th moment of the unrimed snow population's size distribution and m_p is the total unrimed snow mass concentration.

We previously assumed that b_m and b_{mp} are equal, and also that the size distribution of the actual full snow population is the same as if the snow field were comprised only of the pristine mass. Using these assumptions, the b_{mp}th moment of the unrimed snow population's size distribution is equal to the b_mth moment of the full rimed snow population's size distribution, i.e., that the right-hand sides of equations (3.10) and (3.11) are equal. This leads to the relation

$$a_m \; = \; a_{mp} \frac{m}{m_p} \tag{3.12}$$

which gives us an a_m value for the total combined snow field. a_{mp} is the already known empirically obtained value for pristine snow, and both m and m_p are predicted by the model.

We assume that a snow particle's velocity varies linearly with rime mass fraction between the empirically obtained values of unrimed snow and GLS. Since the velocities

of unrimed snow and GLS are described by power laws, they appear as lines on a log-log plot. We assume that the adjusted velocity is also a power law, appearing as a line on the log-log plot, and is just the mass-weighted average of the two lines for pristine snow and GLS. When converted back to a power law, the adjusted constants can be expressed as follows

$$a_v \;=\; \exp\!\left[\left(\frac{m-m_p}{m_g-m_p}\right)\ln(a_{vg}) \;+\; \left(\frac{m_g-m}{m_g-m_p}\right)\ln(a_{vp})\right] \tag{3.13}$$

and

$$b_v \;=\; \left(\frac{m-m_p}{m_g-m_p}\right) b_{vg} \;+\; \left(\frac{m_g-m}{m_g-m_p}\right) b_{vp} \tag{3.14}$$

where a_v and b_v are for the total snow field, a_{vg} and b_{vg} are the a_v and b_v parameters for GLS, and m_p is the mass of the unrimed snow field. m_g is the mass concentration that a population of GLS particles would have if they had the same pristine mass as the actual snow population, obtained with (3.9):

$$m_g = a_{mg}\, M(b_{mg}) \tag{3.15}$$

where m_g is the hypothetical mass concentration of GLS, a_{mg} is an empirically derived value for the mass-diameter power law for GLS, b_{mg} is assumed to be the same as the known value of b_{mp} (recall that b_m is assumed to be independent of rime mass), and $M(b_{mg})$ is the b_{mg}th moment of the total snow population's size distribution.

Fig. 3.1 shows a sample plot of the mass-weighted mean fall velocity resulting from equations (3.6), (3.13), and (3.14), with the "pristine snow" power law constants taken from Locatelli and Hobbs (1974) values for unrimed dendrites, and the GLS values also taken from Locatelli and Hobbs (1974). Tracing a path rightward along the x-axis from the origin to the red line yields fall velocity values that represent those produced by current microphysics schemes, since they treat all snow as pristine. Following the red line toward the upper left preserves the total mixing ratio of the snow field, but increases riming mass fractions (RMFs), so the fall velocities increase as a result.

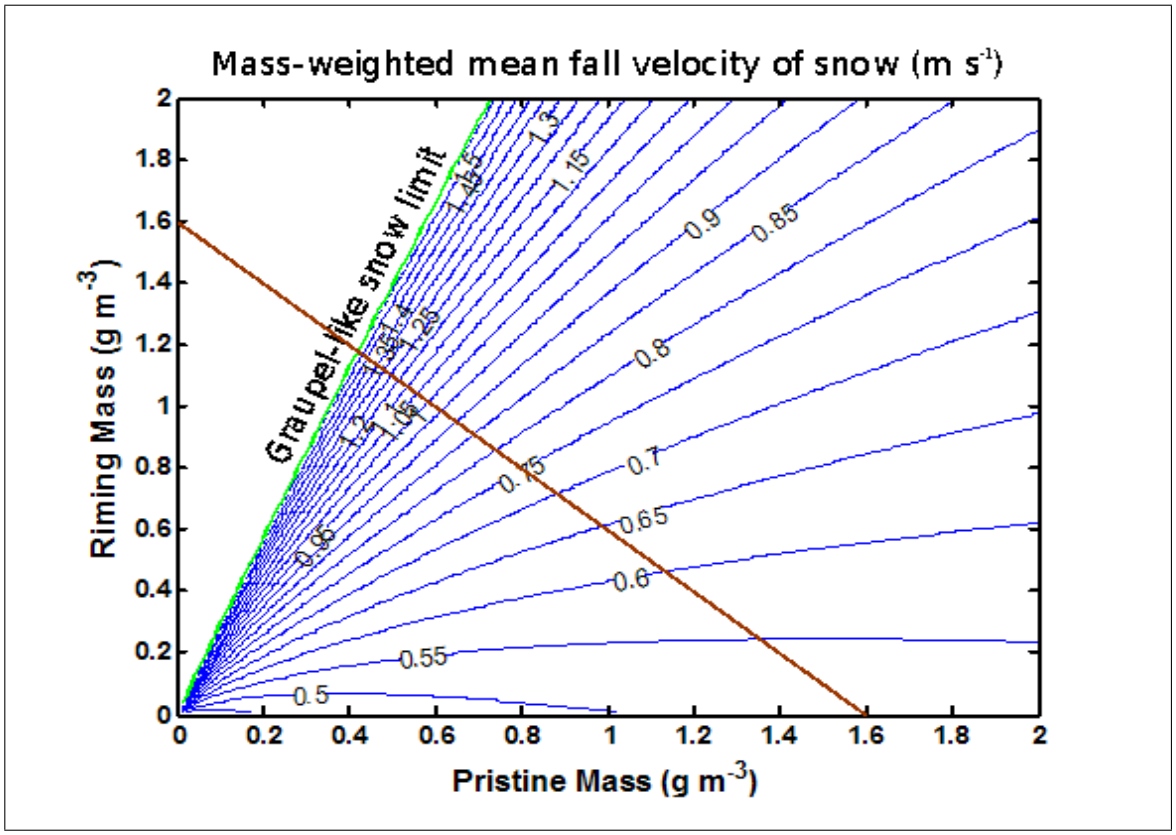

Figure 3.1: Mass-weighted mean fall velocities for dendrites as a function of their rime mass and pristine mass. Lines of constant mass-weighted mean fall velocity appear as blue lines. The red line represents a line of constant total snow mixing ratio. The green line represents the maximum velocity snow can achieve without being converted to graupel.

The line labeled "graupel-like snow limit" represents the maximum mass-weighted fall speed that snow can achieve without being converted to graupel.

The Thompson scheme, like many six-class bulk microphysics schemes, includes graupel among its species of water. Graupel describes hydrometeors that have rimed so heavily that they are almost entirely comprised of rime. Within the Thompson scheme, the transformation of rimed snow to graupel occurs when riming becomes the locally dominant growth process, having an instantaneous growth rate five times greater than deposition's. When this occurs, a portion of the rime mass that would ordinarily transfer from the cloud water category to snow is instead immediately redirected to graupel. While this correctly recognizes the importance of the riming process in graupel production, it limits graupel's formation to moments of instantaneous heavy riming, rather than responding to an accumulation of rime over time.

The riming prediction scheme provides information that makes it possible to improve upon this method. With separate equations for the mixing ratio of rime mass and pristine mass, determining rime's relative abundance need not depend upon the present rate of riming. Instead, this value can be calculated directly from the rime and pristine mass mixing ratios, allowing the model to base initial graupel production upon the relative amount of rime mass accumulated.

In the literature, the GLS description refers to a snow particle that has become sufficiently rimed as to lose its habit-distinguishing features. Therefore, it seemed reasonable to choose the RMF associated with GLS as the RMF threshold that triggers the "autoconversion" of snow to graupel. However, for a given accumulation of rime mass, some of the crystal population would be less heavily rimed, and some more. A more realistic scheme, therefore, would autoconvert a small portion of rime mass before the RMF reached that of GLS. Consequently, we chose a threshold of 80% of the RMF for GLS, beyond which any excess rime mass would be autoconverted to graupel.

Choosing a threshold based on the RMF of GLS requires knowledge of the total

mass concentration and rime mass concentration that a hypothetical population of GLS particles would have if it had the same pristine mass as the actual snow population. The total mass concentration of such a population was already calculated with (3.15). The rime mass concentration is just

$$m_{gr} = m_g - m_p \tag{3.16}$$

where m_{gr} is the rime mass concentration of the hypothetical GLS field, and m_p is the predicted pristine snow mass. Finally, the RMF for the hypothetical GLS population is given by

$$\mathrm{RMF}_{\mathrm{GLS}} = \frac{m_{gr}}{m_g} \tag{3.17}$$

The new method of initial graupel production, which we refer to as autoconversion of snow to graupel, replaces the term in the unaltered Thompson scheme referred to as production of graupel due to snow collecting cloud water.

3.3.2 Experimental Setup

To evaluate the effects of adding riming prediction to a microphysics scheme, we chose to run model simulations of various resolutions, comparing the Thompson scheme, which acted as our control, with the riming prediction scheme. Initially, we intended to use habit prediction within both the control and riming prediction schemes, but considering the inability of the habit prediction to correctly produce observed habits, and that the negative impact of poor habit prediction might well overshadow the effects of riming, we decided to turn off habit prediction in both the control and riming prediction experiments, opting instead for the behavioral characteristics of a hybrid of unrimed dendrites and cold-type particles type (as determined from our own observations) for our "pristine" power law constants (see column 2 of Table 3.1) and the behavior of GLS reported in Locatelli and Hobbs (1974) for our GLS power law constants (see column 3 of Table 3.1). We used a hybrid of dendrites and cold-type

particles based on their dominant occurrence in our climatology. We also turned off a simple attempt that Thompson installed in his scheme to accelerate rimed snow particles, which increased fall speeds of snow proportional to local riming growth. The riming boost for fall speed was tested and found to increase fall speeds only a very small amount relative to our method.

Parameter	Dendrites / Cold-type Hybrid	GLS	Units
a_m	0.02283	0.1177	$\frac{\mathrm{Kg}}{\mathrm{m^{b_m}}}$
b_m	2.06	2.1	unitless
a_v	4.1061	7.61	$\frac{\mathrm{m^{1-b_v}}}{\mathrm{s}}$
b_v	0.265	0.28	unitless

Table 3.1: Power law parameters for pristine snow and graupel-like snow used in the riming prediction model simulation.

Special circumstances forced us to limit the scope of our analysis to just one of the meteorological cases (February 6, 2008) used to test the habit prediction scheme. A discovery late in the research process of an incorrect constant in our code rendered many of our case study experiments invalid. After this discovery, we focused on the single case study, with emphasis on fully understanding the behavior of the scheme and confirming reasonable behavior.

3.3.3 Analysis And Results

The storm system of February 6, 2008, was in many ways typical of landfalling extratropical cyclonic storms in the Pacific Northwest. A well-developed surface low pressure center located in the Gulf of Alaska moved slowly toward the northeast, and a weaker occluded frontal band passed onshore and over the Olympic and Cascade Mountains. Prior to and during the passage of the frontal band, low-level flow was

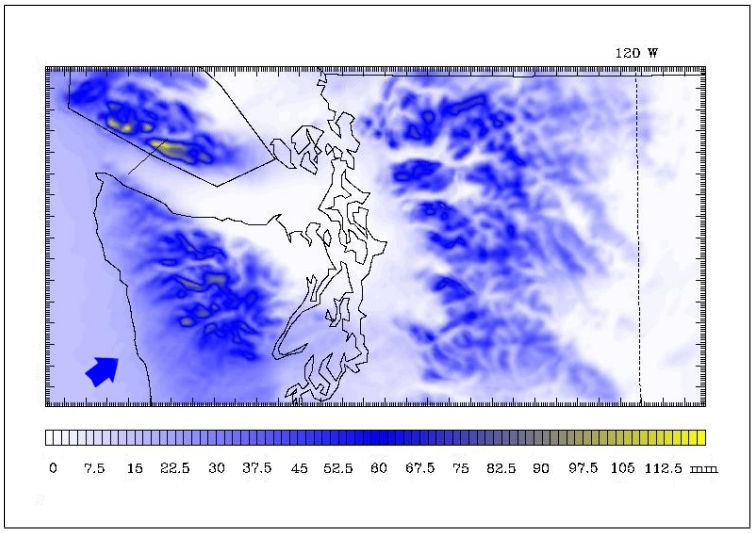

Figure 3.2: Total accumulated precipitation in the control scheme for the February 6-7, 2008 case. The cross-section studied in depth appears as a black line in the vicinity of southwestern Vancouver Island. The blue arrow represents the storm-mean and area-mean wind flow at 850 hPa.

from the south, veering to southwesterly aloft. Following the surface frontal passage was a period of six hours of slowly diminishing post-frontal orographic precipitation with more westerly flow.

Examining the total accumulated precipitation over the course of the entire storm (see Fig. 3.2) from the 1.33 km. domain (accumulated from 12Z UTC Feb. 6 to 12Z UTC Feb. 7), we notice the relatively common pattern of enhanced precipitation over the mountainous regions, and, more specifically, over the Cascades, the Olympics, and Vancouver Island. Looking at the difference in precipitation between the control scheme and the riming prediction scheme over the course of the entire storm (see Fig. 3.3), many areas of significant differences can be seen. These differences range from 10% to 30% of the total collocated precipitation from the control run. In many locations, particularly over the Olympics, but to a lesser degree elsewhere, one can see a general deficit of precipitation both windward and leeward of of the crest, with a

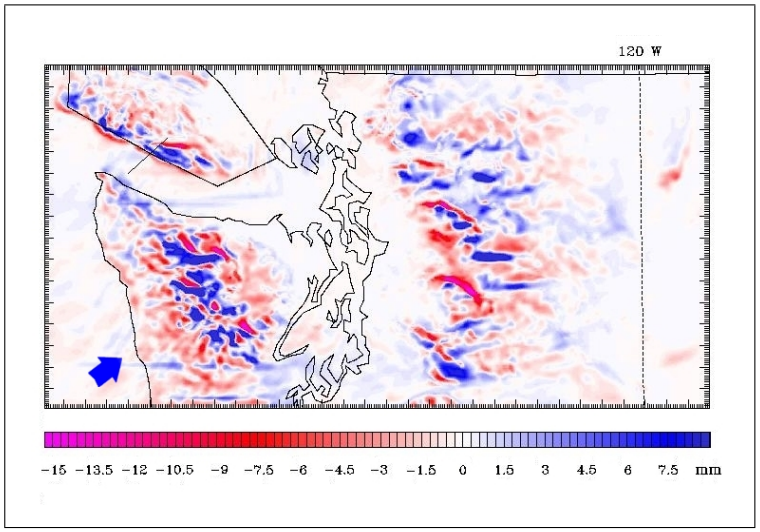

Figure 3.3: The difference in total accumulated precipitation between the control scheme and riming prediction scheme for the February 6-7, 2008 case. Positive values indicate a net increase in precipitation for the riming prediction scheme, while negative values indicate a net loss. The cross-section studied in depth appears as a black line in the vicinity of southwestern Vancouver Island. The blue arrow represents the storm-mean and area-mean wind flow at 850 hPa.

surplus directly over the crest. This pattern is also evident to a lesser extent over the coastal mountains of Vancouver Island. As will be the convention for the remainder of plots, areas of blue (progressing to yellow) represent an increase in the quantity being presented (e.g. accumulated precipitation) for the riming prediction scheme relative to the control scheme, and areas of red (progressing to magenta) represent a relative decrease. Also, because of boundary-related artifacts in the southern part of the domain that were clearly parallel to either the western or southern boundary, these figures show a subset of the innermost domain.

Visible on both of these precipitation plots is a line, extending from the Strait of San Juan de Fuca to the southwestern portion of Vancouver Island, which represents the cross-section we chose to examine in greater depth at the specific time of 17.4 hours into the model run. We chose this particular combination of cross-section and time because at that time, the oncoming wind was perpendicular to the crest of a nice, bell-shaped ridge on the island, and the location had the added benefit of having no immediate obstructions upstream. Further, the precipitation pattern differences between the two schemes was, at that time and location, reasonably representative of the storm accumulated pattern. In essence, the transect over Vancouver Island represented a "2-D idealized model of opportunity", which we used to probe and understand the behavior of the riming prediction scheme.

In several plots that follow, we present our results in terms of precipitation rate (or precipitation "fluxes", which we use interchangeably) instead of mixing ratios. For falling species in particular, this has the advantage of showing mass in a consistent way, taking fall speeds into account. For example, in a steady state stratiform precipitation situation with a melting layer with no precipitation growth, the precipitation mixing ratio in the snow region is much higher than in the rain region, even though no growth has occurred. There has only been mass divergence as the melting particles accelerate. But precipitation rate is constant across such a melting layer. In essence, precipitation rate gives a clearer picture of growth compared to mixing ratio.

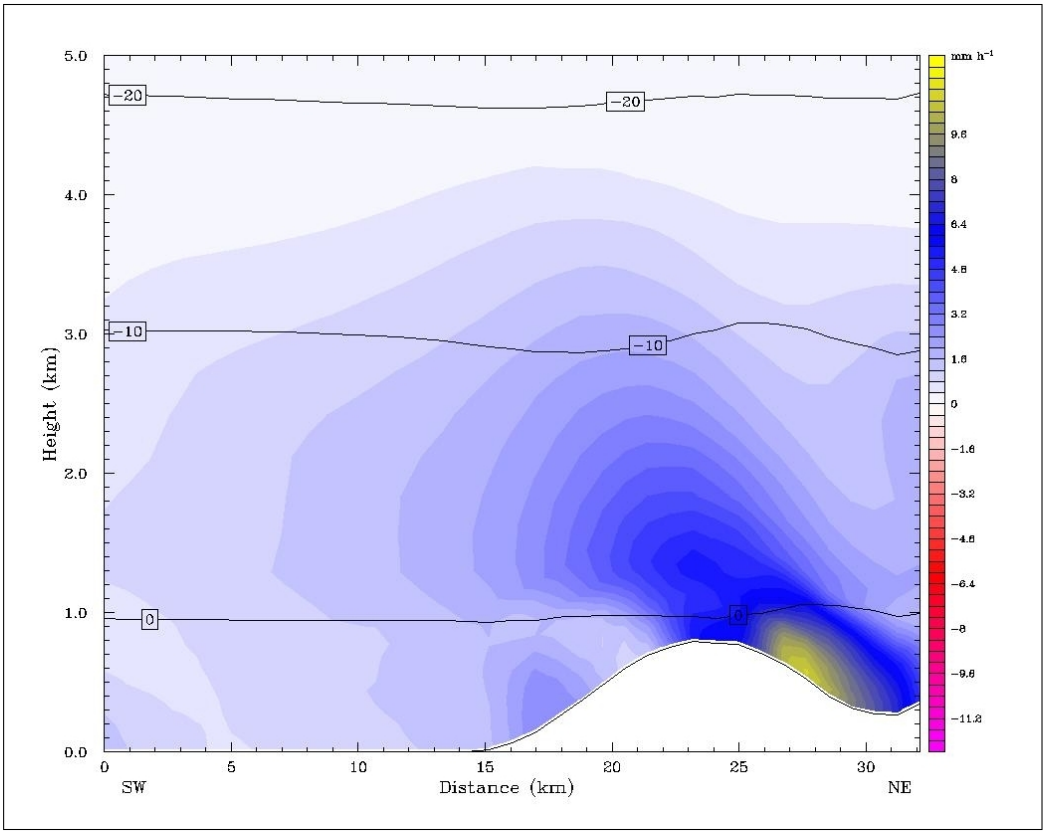

Figure 3.4: A vertical cross-section of instantaneous precipitation rate of the total combined precipitation field over southwestern Vancouver Island for the control scheme 17.4 hours into the model simulation.

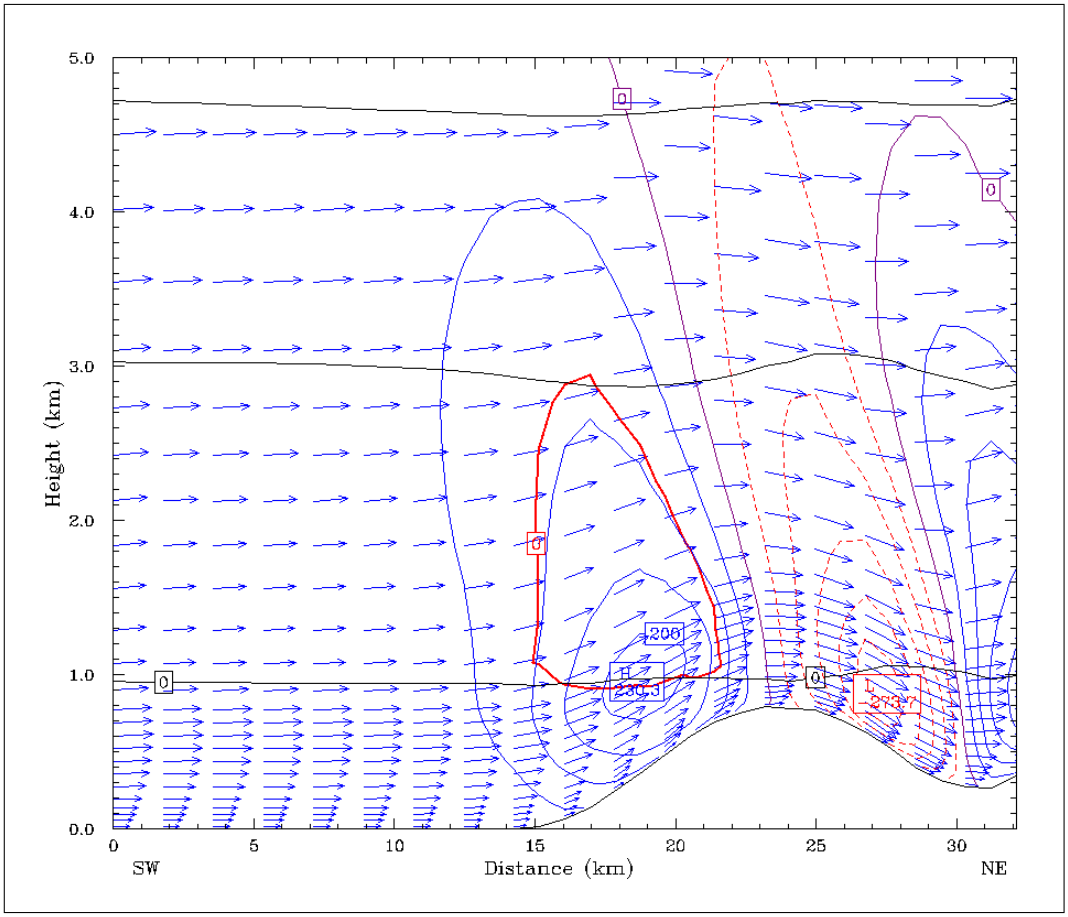

Figure 3.5: Circulation vectors within the plane of the vertical cross-section, contours of vertical air velocity in cm/s (areas of upward velocity in blue, downward velocity in dashed red), and the area of net upward snow velocity (enclosed by the red contour) over southwestern Vancouver Island for the control scheme 17.4 hours into the model simulation.

Looking, first, at the precipitation rate of the total precipitation field (i.e. graupel, snow, and rain) for the control scheme (see Fig. 3.4), there is an area of intense precipitation rate in the vicinity of the crest of the ridge. While in the lee the precipitation rates are greatest, on the windward slope there appears to be a gap in the generally elevated precipitation rates hovering above the ridge. This feature is the result of particularly intense vertical air velocities. That is, the vertical air velocities shown in Fig. 3.5 reach peak upward velocities that are more than twice typical snow fall velocities, resulting in a region, encircled in red, of net upward motion for snow. This of course prevents snow from falling below the melting layer in the vicinity of the strong upward motion. Rain, however, falls much faster than snow, and therefore any rain that forms below the melting level manages to fall to the ground, and in fact, grows by additional collection of cloud water, explaining the local maximum of precipitation on the lower windward slope.

Examining the difference in precipitation rate of the total precipitation field between the control scheme and the riming prediction scheme (Fig. 3.6), five features become distinguishable. Starting at the far windward portion of the ridge, there are five bands alternating between deficits and surpluses of precipitation for the riming prediction scheme. The first two features, (a) and (b), are similar in size, shape, and intensity, together appear to represent a displacement of rain toward the crest of the ridge. They do not appear to be physically connected to differences in precipitation rate above the melting level, although ultimately, they must be, considering that the riming prediction scheme only changes processes at subfreezing temperatures. Perhaps there is a small but important difference in the snow that just barely makes it through the melting level before the large vertical velocities loft all snow up the slope. In any event, this difference is a testament to the inherent complexity and nonlinearity in microphysical schemes, in that unanticipated results can occur that are seemingly unrelated to the changes made.

The remaining three features, an area of increased precipitation at the crest strad-

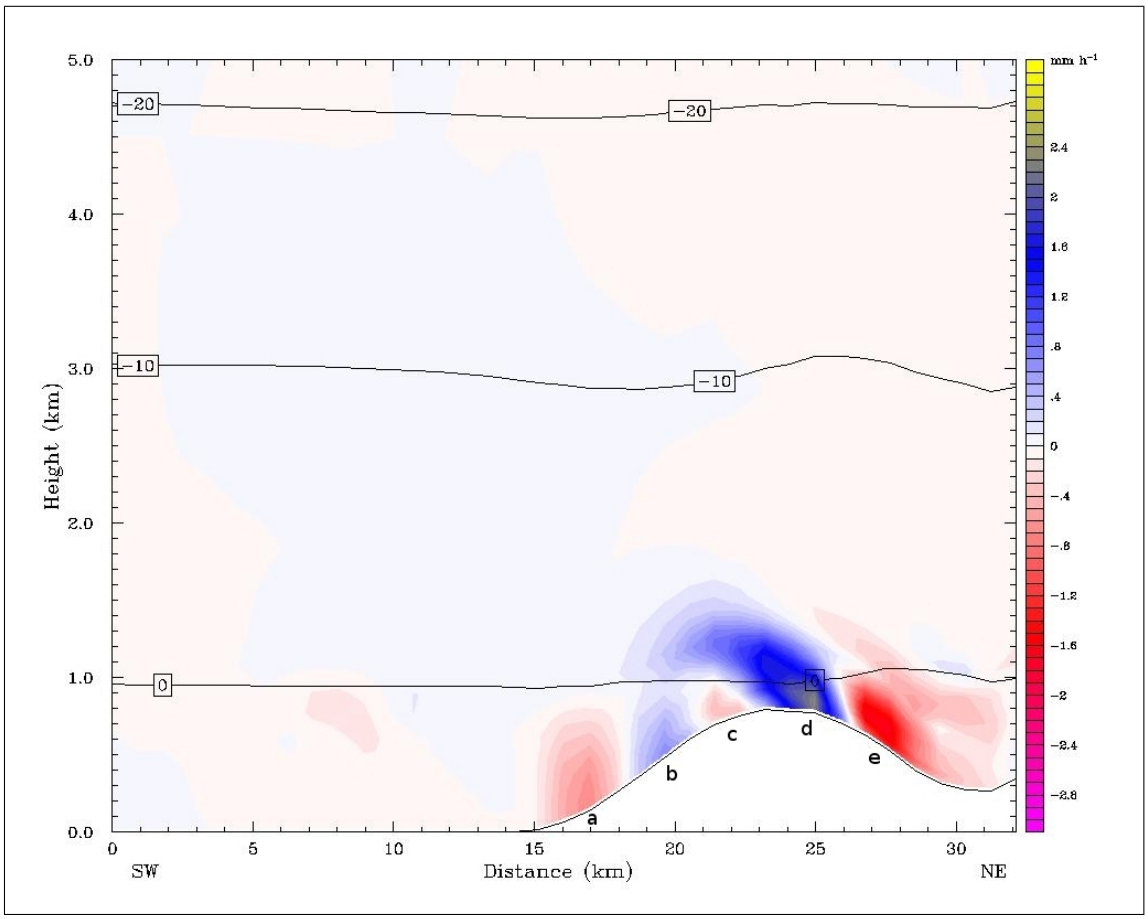

Figure 3.6: A vertical cross-section of the difference in instantaneous precipitation rate of the total combined precipitation field between the control scheme and riming prediction scheme over southwestern Vancouver Island 17.4 hours into the model simulation. Positive values indicate a net increase in the instantaneous precipitation rate for the riming prediction scheme, while negative values indicate a net loss.

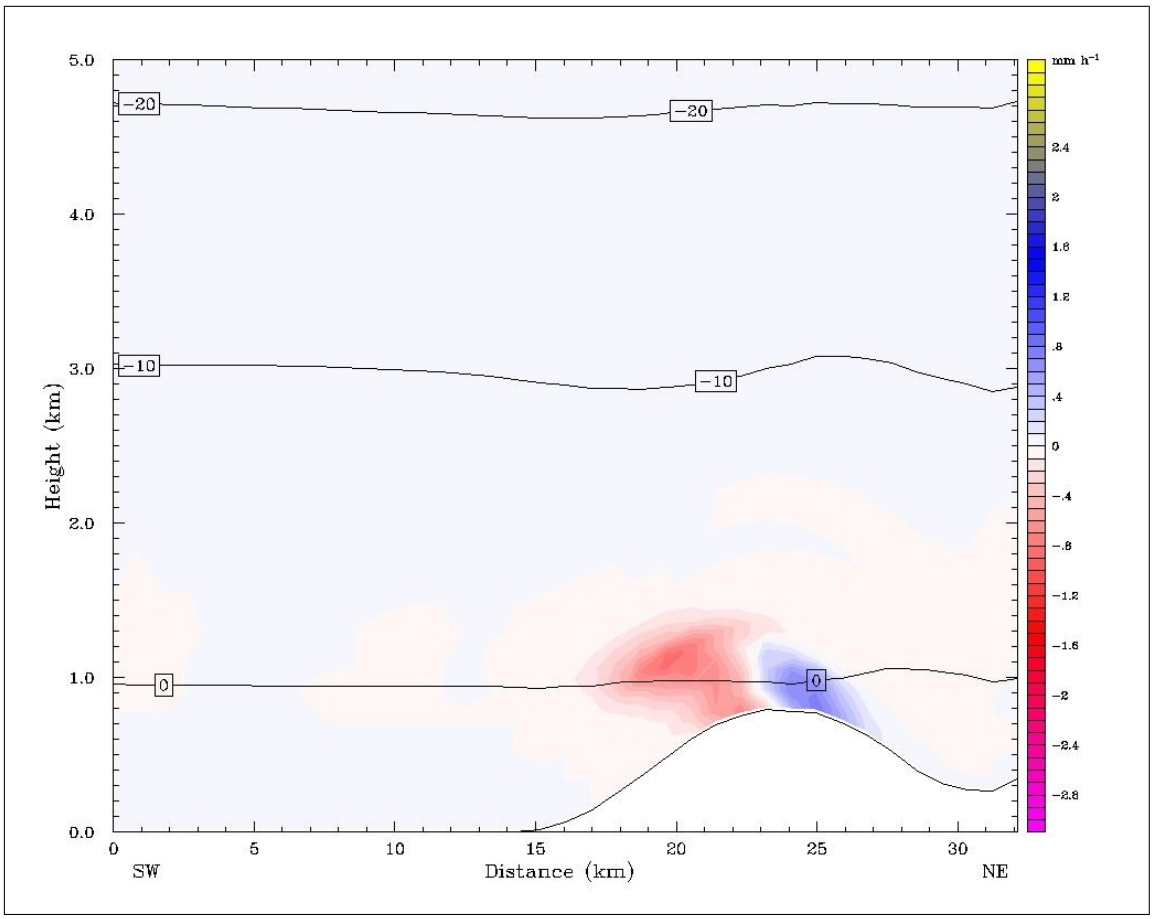

Figure 3.7: A vertical cross-section of the difference in instantaneous precipitation rate of the graupel precipitation field between the control scheme and riming prediction scheme over southwestern Vancouver Island 17.4 hours into the model simulation. Positive values indicate a net increase in the instantaneous precipitation rate for the riming prediction scheme, while negative values indicate a net loss.

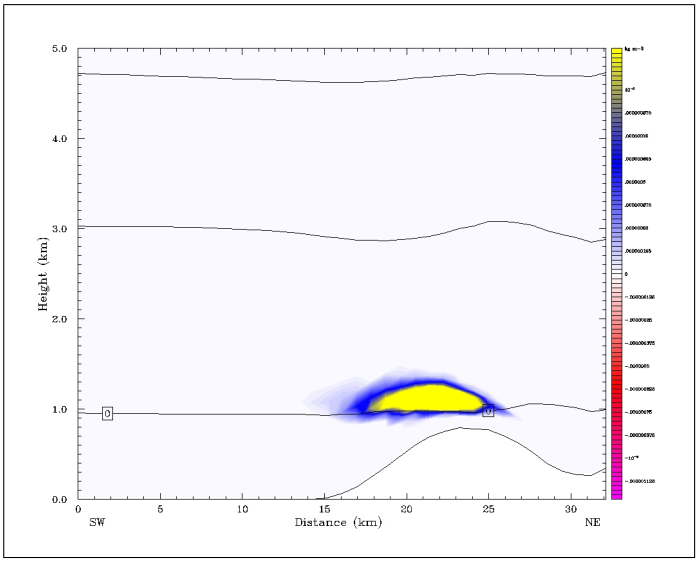

Figure 3.8: A vertical cross-section showing the autoconversion to graupel of snow over southwestern Vancouver in the control scheme Island 17.4 hours into the model simulation.

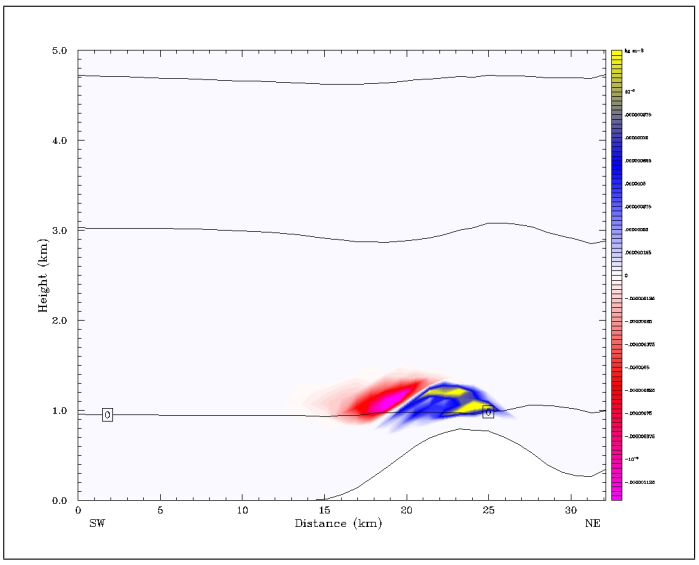

Figure 3.9: A vertical cross-section showing the difference in the autoconversion to graupel of snow between the control scheme and riming prediction scheme over southwestern Vancouver Island 17.4 hours into the model simulation. Positive values indicate a net increase in the amount of autoconversion for the riming prediction scheme, while negative values indicate a net loss.

dled by an area of decreased precipitation on either side, represent two separate phenomena. The first of these phenomena involves features (c) and (d) only, and can be better understood by looking at the portion of those features caused by differences in the graupel precipitation rate field. As Fig. 3.7 shows, graupel precipitation rates within the riming prediction scheme decrease just windward of the crest and then increase slightly leeward of the crest, suggesting that graupel has been displaced leeward. The mechanism responsible becomes clearer by looking at the production of graupel. Figure 3.8 shows the area of graupel production within the control scheme to be just windward of the ridge crest. The difference in graupel production between the two schemes (see Fig. 3.9), shows a large deficit of graupel production becoming a large surplus as one moves leeward. This delay in graupel production for the riming prediction scheme is a direct result of the way that riming prediction transfers mass to graupel. Instead of instantly converting rime mass to graupel when the rate of riming is large, it converts it when a sufficient amount of rime mass has accumulated, holding the rime mass in snow longer. Further, once the conversion to graupel of rimed snow has begun and the snow remains in a densely rimed state, less new riming is required to convert rime mass to graupel, helping to explain the increase in graupel production directly above the ridge crest.

The second of the phenomena involves only features (d) and (e) from Fig. 3.6. Ultimately, to explain why these features exist, we need to consider what is happening with the snow field. Unfortunately, doing so is complicated by the existence of the melting level, forcing us to examine the combination of snow and rain precipitation rates. As it happens, nearly all the rain comes from melting snow (graupel is less prevalent than snow and also falls to the surface largely unmelted). Thus, what appears in Fig. 3.10, the difference in snow and rain precipitation rates between the control scheme and riming prediction scheme, is almost entirely the result of snow processes. The exception here is along the windward slopes, where we see the warm rain feature discussed previously. Above the freezing level and extending down to the

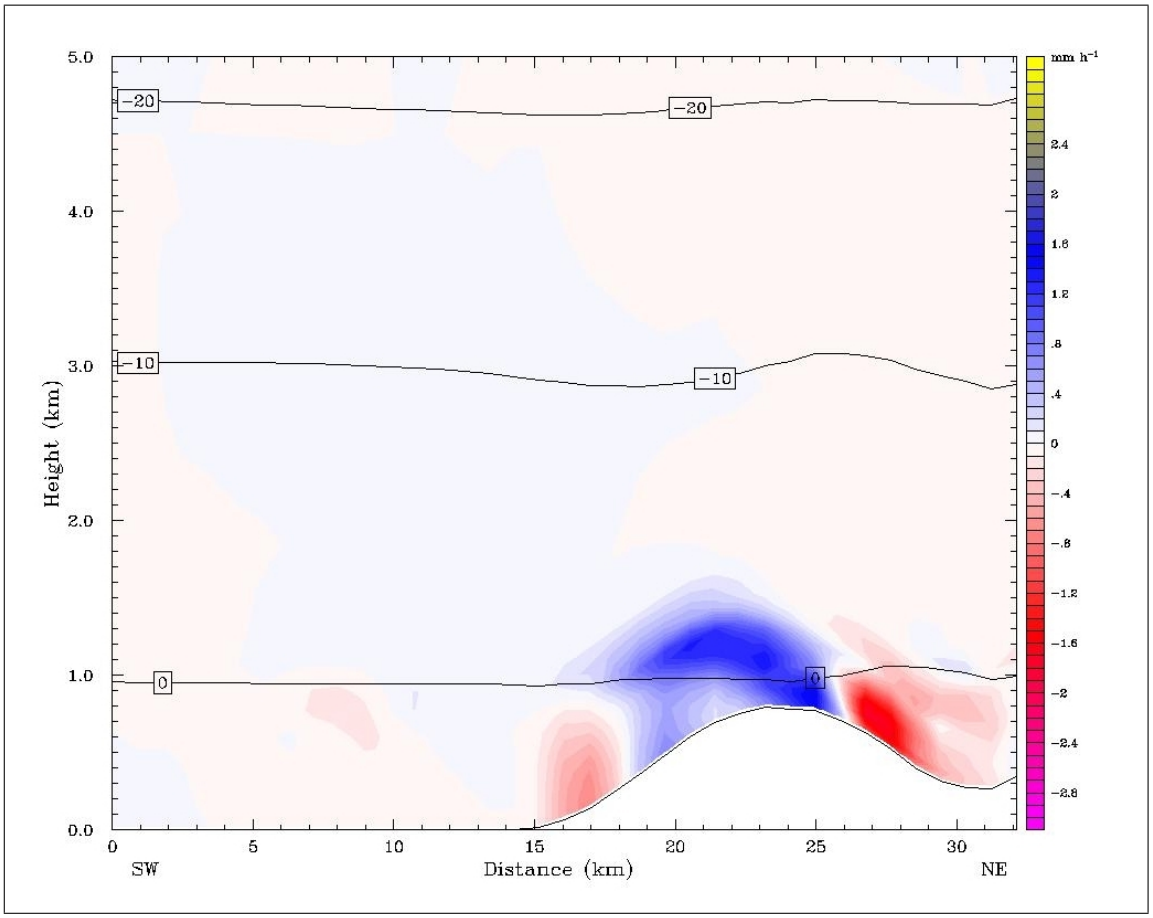

Figure 3.10: A vertical cross-section of the difference in instantaneous precipitation rate of the combined snow and rain precipitation field between the control scheme and riming prediction scheme over southwestern Vancouver Island 17.4 hours into the model simulation. Positive values indicate a net increase in the instantaneous precipitation rate for the riming prediction scheme, while negative values indicate a net loss.

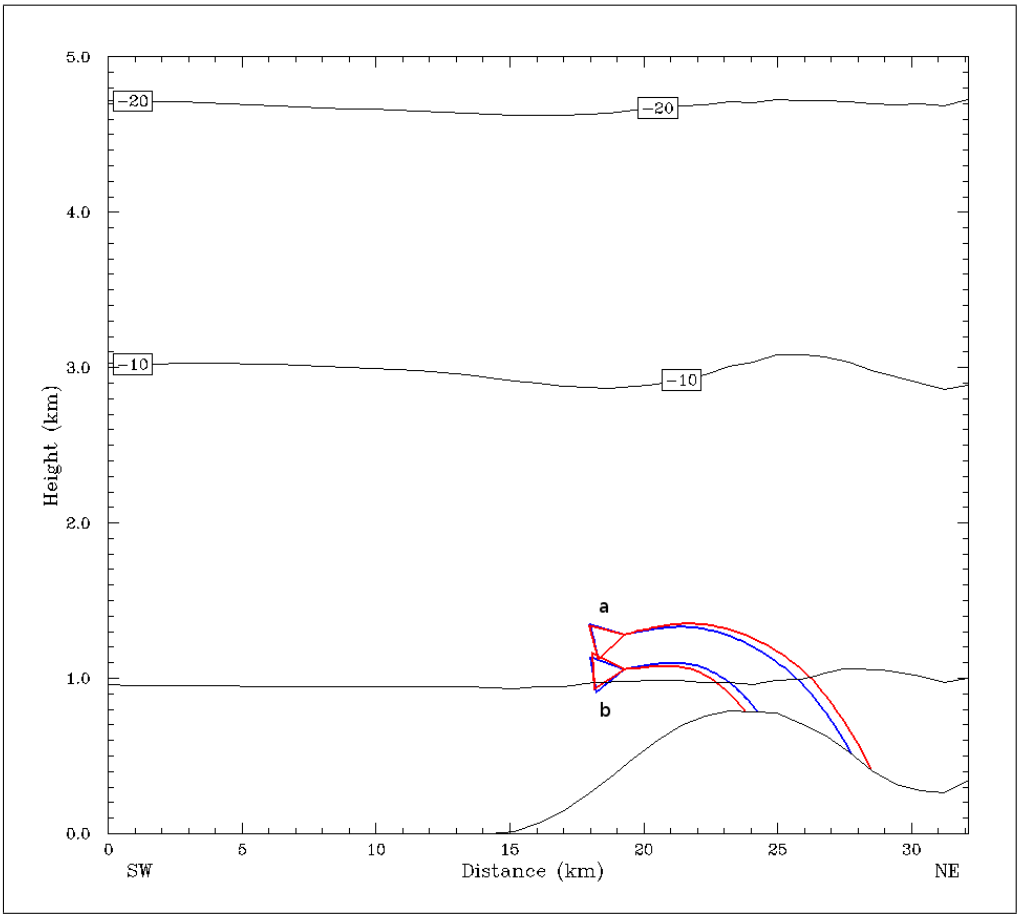

Figure 3.11: A vertical cross-section showing trajectories of particles representing the combined mass-weighted precipitation fields of the control scheme (in red) and riming prediction scheme (in blue) over southwestern Vancouver Island beginning at 17.4 hours into the model simulation. The upper set of trajectories (a) originate in a region that is more heavily influenced by snow, whereas the lower set of trajectories (b) originate in an area more heavily influenced by the presence of graupel.

ridge crest we see an area of increased precipitation rates, while further leeward, we see an area of decreased precipitation rates. The region above the freezing level can be explained by the mechanism discussed previously in which snow holds on to rime mass longer, temporarily increasing the amount of snow mass aloft before being converted to graupel. Nearer the surface, the juxtaposition of the regions of surplus and deficit precipitation rates once again suggests a displacement, in this case windward toward the crest. This pattern could be accounted for if snow particles were falling faster in the riming prediction scheme, which, as it turns out, they do. This can be seen in Fig. 3.11, in which hydrometeor trajectories representing the entire mass-weighted precipitation field are shown. The initially lower trajectory is subject to the delay in graupel production previously discussed. The riming prediction trajectory falls slower because it behaves more like rimed snow than like graupel, and is shifted eastward. Meanwhile, the initially higher trajectories show that riming prediction causes the particle particle to fall faster than its control scheme counterpart, because in this location is behaves more like rimed snow instead of like unrimed snow, essentially displacing its landing location crestward. The overall result of both processes is that with riming prediction, precipitation is "squeezed" toward the crest (or just slightly leeward of the crest) from both the windward and leeward slopes.

In addition to understanding those mechanisms that clearly lead to changes in ground precipitation, we wanted to examine other noteworthy differences between the two schemes whose net effects might have been less obvious. More specifically, we found that assuming rime mass doesn't affect a snow crystal's diameter had interesting consequences. These consequences can be seen by looking at several production terms, starting with deposition in the control scheme (see Fig. 3.12). From the plot, we see that deposition is strongest aloft, especially along the upper boundary of water saturation (the upper and lower boundaries of water saturation appear as thick black lines), while sublimation occurs leeward of the ice saturation boundary (appearing as a vertical gray line directly above the ridge crest). Looking at the difference in deposi-

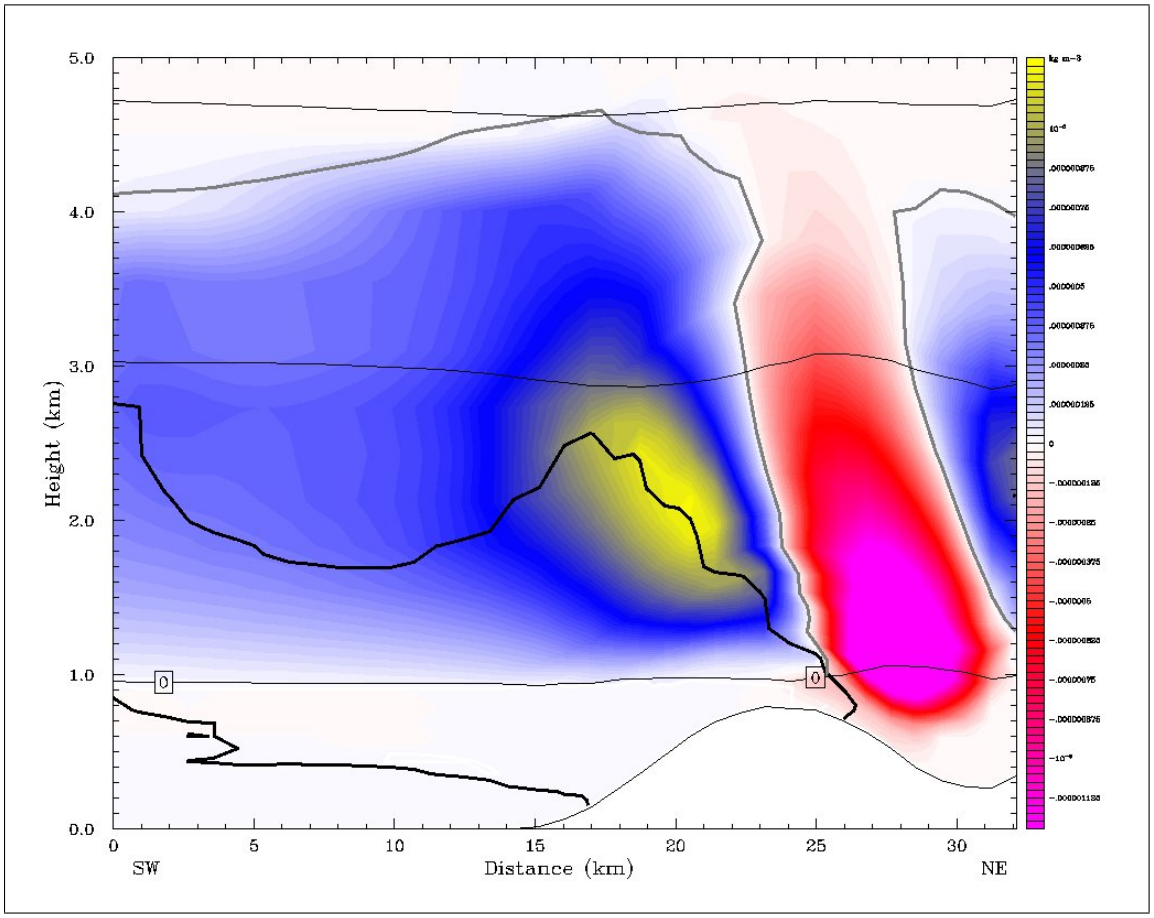

Figure 3.12: A vertical cross-section showing deposition and sublimation over southwestern Vancouver Island in the control scheme 17.4 hours into the model simulation. Areas in blue and yellow denote the occurrence of deposition, while red and magenta denote sublimation. The upper and lower thick black lines represent the upper and lower boundaries of water saturation, respectively. The thick gray lines represent the boundary between ice supersaturation (generally coinciding here with the blue region) and ice subsaturation (generally coinciding with the region in red).

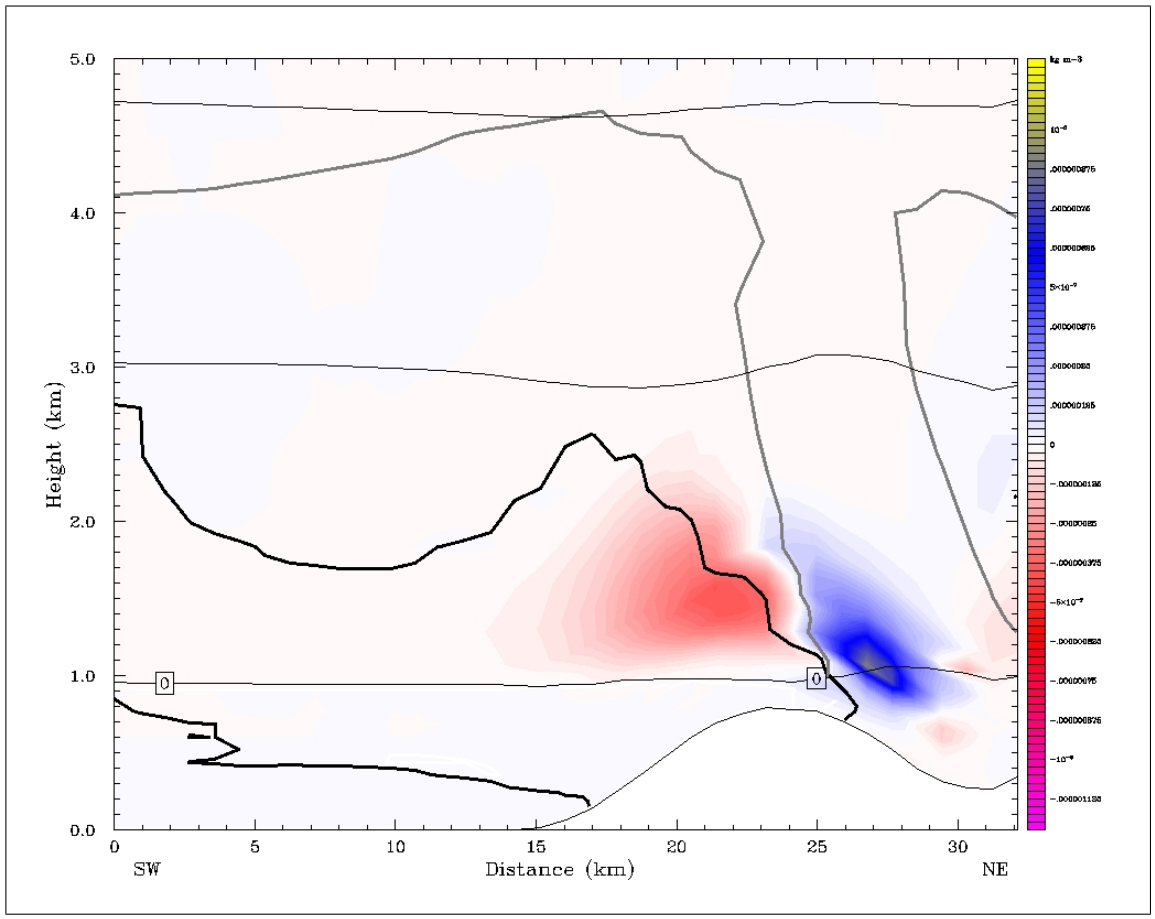

Figure 3.13: A vertical cross-section showing the difference in the deposition and sublimation between the control scheme and riming prediction scheme over southwestern Vancouver Island 17.4 hours into the model simulation. Red areas indicate a net decrease in the amount of depositional growth for the riming prediction scheme, while blue areas indicate a net decrease in sublimation. The thick black and gray lines are as described in Fig. 3.12.

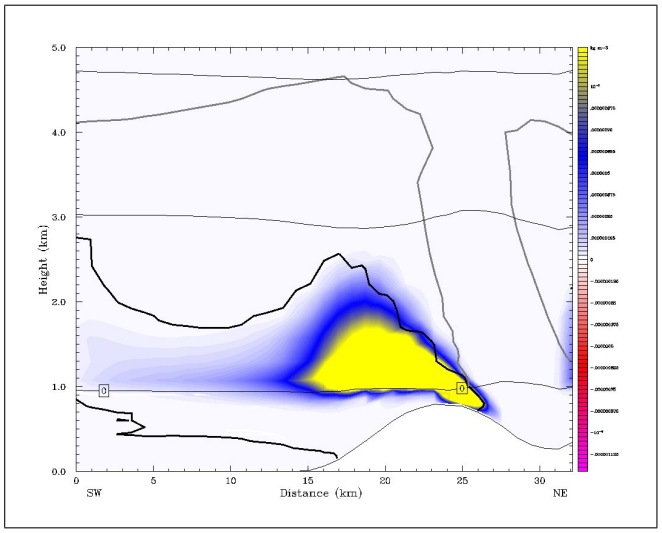

Figure 3.14: A vertical cross-section showing riming over southwestern Vancouver Island in the control scheme 17.4 hours into the model simulation. The thick black and gray lines are as described in Fig. 3.12.

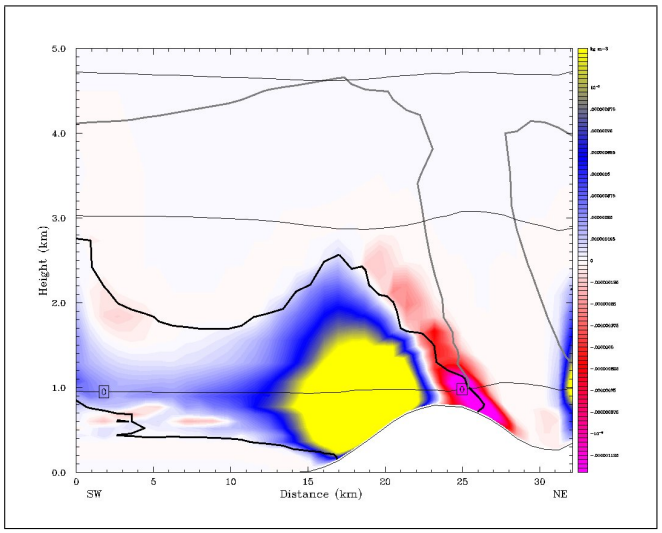

Figure 3.15: A vertical cross-section showing condensation and evaporation of cloud water over southwestern Vancouver Island in the control scheme 17.4 hours into the model simulation. Areas in blue and yellow denote the occurrence of condensation, while red and magenta denote evaporation. The thick black and gray lines are as described in Fig. 3.12.

tion between the control scheme and the riming prediction scheme (see Fig. 3.13), we notice an area of decreased deposition whose upper boundary is located in what was the lower portion of strongest deposition, with the decrease in deposition becoming even more pronounced farther down, and we see area of decreased sublimation in the lee of the ice saturation line. These differences are understandable in the context of how the riming prediction is formulated. That is, when riming occurs, riming prediction, unlike the control scheme, adds mass to the snow field without affecting its size distribution. This results in a smaller mass-weighted mean diameter for an equivalent amount of accumulated rime mass. Within the microphysics scheme, having relatively smaller diameters translates into having less surface area available to deposition, in essence retarding it. Recognizing that the relative suppression of deposition requires the presence of riming, we see from Fig. 3.14 that riming does indeed exist in the vicinity of the depositional deficit. In fact, comparing Figs. 3.12, 3.13, and 3.14, we see that the area of greatest overlap between riming and depositional growth is where the depositional deficit is greatest. If we consider the region of reduced sublimation in Fig. 3.13, this too makes sense since the rate of sublimation also depends upon the amount of surface area available, and therefore on the mean diameter.

This result has further consequences. From Fig. 3.15, we see that condensation within the control scheme is happening where we would expect, within the region that has reached water saturation. While a small region of evaporation appearing within the region of water saturation might at first seem out of place, this region is located where the winds near the crest have begun their descent and only the evaporation of the remaining cloud water temporarily maintains the humidity at level of saturation. If we look at the difference in condensation between the two models (see Fig. 3.16), we see that an area of increased condensation exists in virtually the same location as the deficit of deposition, and we see an area of increased evaporation near the water saturation boundary. This is what we would expect since a decrease in deposition would lead to the greater availability of moisture for condensation, and the resulting

extra cloud water would leave additional moisture available to evaporation.

Lastly, we examine the difference in riming between the control scheme and the riming prediction scheme. From Fig. 3.17 we see an area of suppressed riming sandwiched between regions of increased riming above and below. Attempting to understand the underlying causes of this pattern is quite difficult because of the number of highly variable factors playing a role, including size distribution, snow and graupel fall speeds, and differences in both cloud water and snow fields. Some of these factors also have notable feedbacks. For example, the efficiency of collection would likely be affected by differences between the two schemes in the mean particle diameter or in particle fall velocities.

However, despite these complexities, upon further inspection, a few salient points become clear. First, an excess of cloud water exists from the midpoint of the red band upward. Because the intensity of riming is related to the amount of available liquid cloud water, the partial collocation of enhanced cloud water with enhanced riming probably partially explains the enhanced riming (relative to the control). Countering this effect in the vicinity of the red band is a decrease, relative to the control, in the mean snow particle diameter. This difference is going to be most prominent where riming is most active (Fig. 3.14), since differences in mean diameter are caused by the riming prediction's assumption that particle diameters remain unaffected by the riming process. Finally, as one nears the freezing level, there is a return to excess riming. While there is a deficiency in cloud water here, relative to the control scheme, the absolute presence of cloud water is quite large. When considering that snow is nearly non-existent in this region (recall that net vertical snow velocities are actually upward in this region (see Fig. 3.5), giving little opportunity for snow growth so close to the freezing level), differences in cloud water become unimportant. That is, the factor limiting riming is not the lack of rime particles, but the lack of snow particles to collect them. Therefore, even a small absolute difference in the snow field can cause a large relative difference in riming.

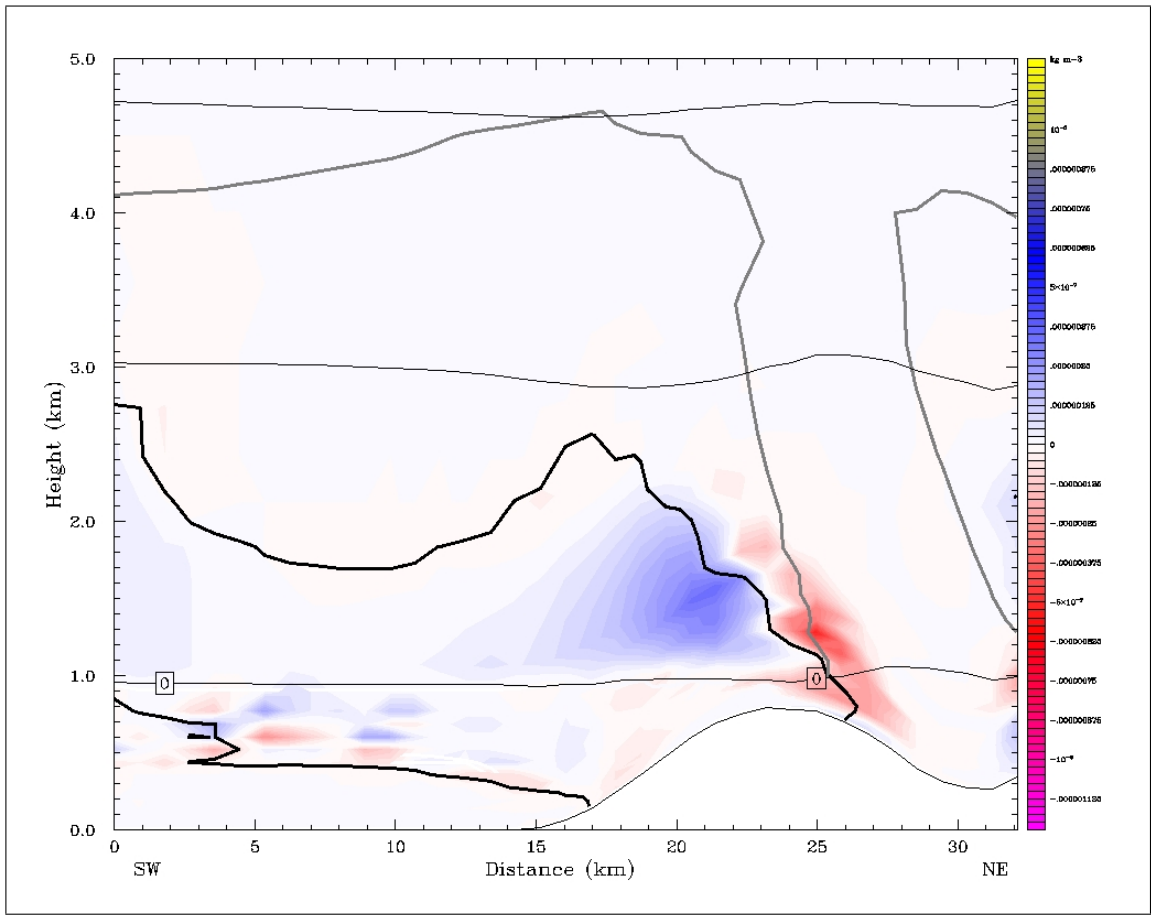

Figure 3.16: A vertical cross-section showing the difference in the condensation and evaporation between the control scheme and riming prediction scheme over south-western Vancouver Island 17.4 hours into the model simulation. Blue areas indicate a net increase in the amount of condensation for the riming prediction scheme, while red areas indicate a net increase in evaporation. The thick black and gray lines are as described in Fig. 3.12.

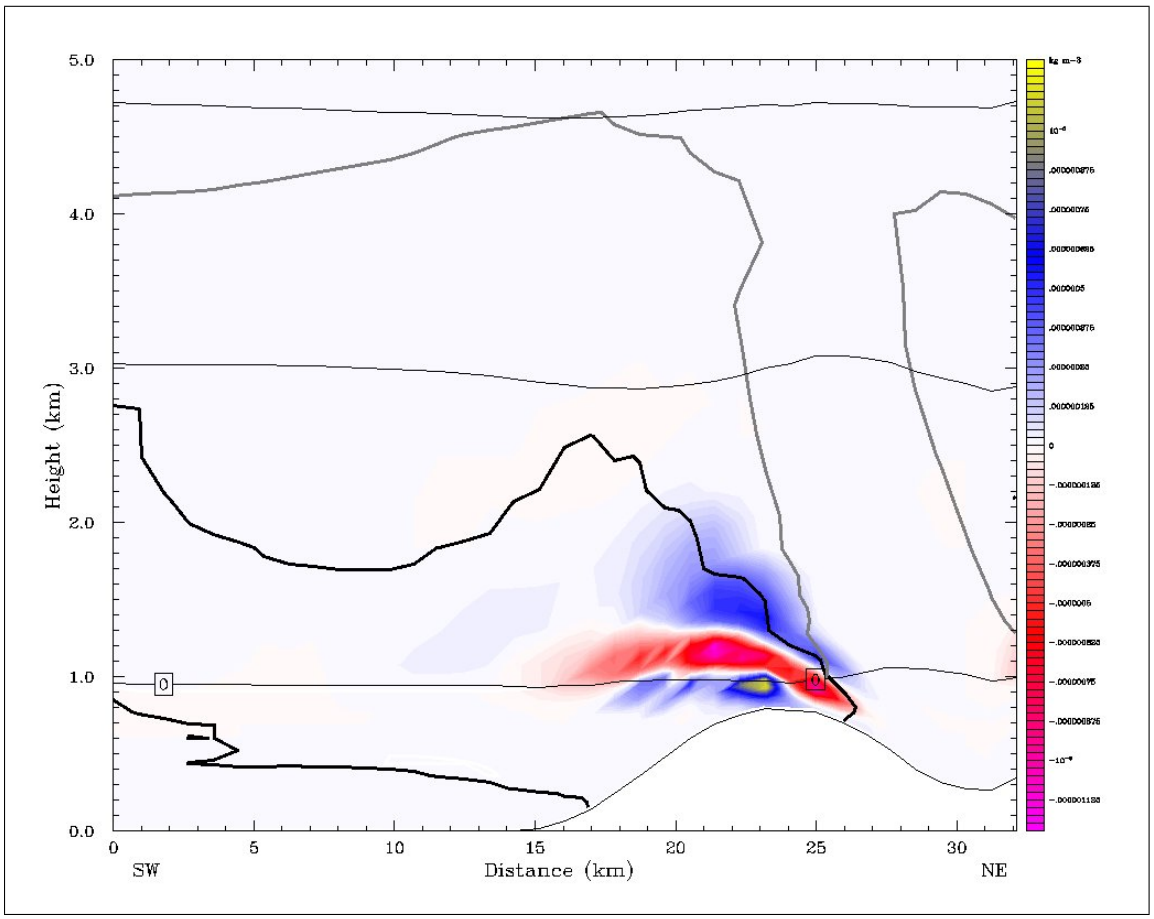

Figure 3.17: A vertical cross-section showing the difference in riming between the control scheme and riming prediction scheme over southwestern Vancouver Island 17.4 hours into the model simulation. Blue and yellow areas indicate a net increase in riming for the riming prediction scheme, while red and magenta indicate a net decrease. The thick black and gray lines are as described in Fig. 3.12.

3.3.4 Summary of Riming Prediction

The riming prediction scheme behaves in a stable and physically understandable manner. Behaviors that were anticipated, namely, longer retention of rime mass in the snow field, the delay in production of graupel, and the acceleration of snow fall speeds due to riming, were seen in the difference fields with the control simulation. This effort represents a first step in the proper representation of rimed snow in bulk microphysical schemes. Next steps include comparison of the scheme with observations like those described in Chapter 2 of this study, and testing and refinement of the assumptions and settings that were required to close the equation set.

Chapter 4
CONCLUSIONS

The present study was intended to address two areas of cloud microphysics: the observed physical characteristics of snow particles and the representation of snow particles within the bulk cloud microphysical schemes used in numerical weather prediction models.

4.1 Observational Data Set

Previous efforts to collect observational data on particle habit and other related quantities have either emphasized the detailed observation of individual particles and their characteristics or the acquisition of statistics on the bulk properties of precipitation by acquiring very large samples, usually at the expense of the other.

The intent of this study was to create a snow-focused observational data set that was robust in its variety of measured parameters, level of detail, and duration. With certain observations, we favored a bulk approach, as with particle fall velocity and size, precipitation rate, and snow depth measurements. With other observations, we favored a more detail oriented approach, as when examining the structural characteristics (i.e. habit type and degree of riming) or population characteristics (i.e. mass-fractional habit makeup) of smaller samples of falling snow particles.

Observations were taken over the winters of 2006-07 and 2007-08, in the Cascades of central Washington. During this time, approximately 60 storms were observed and over 1300 measurements made.

Analysis of the particle fall speed data set yielded the following conclusions:

- Fall speeds of dendrites increase dramatically with increased riming, in contrast

to a recent study.

- Fall speeds of needles and cold-type crystals appear to be less affected by increased riming.

- Rimed dendrites fall fastest, followed by cold-type crystals and then needles, while unrimed dendrites fall the slowest.

We also carried out a climatological study of the particle type makeup of all the frozen precipitation that fell at our observing sites in the Cascade Mountains during the entire 2-year study. This climatology yielded the following conclusions:

- Particles consisting primarily of rime made up 27% of the total mass of all observed hydrometeors, with graupel-like snow accounting for 21% and graupel 6% indicating the importance of riming growth.

- "Unknown" or unidentifiable crystals made up less than 1% of the total observed mass, suggesting that particles examined in sufficient detail are nearly all identifiable.

- Dendrites were the habit most frequently observed, making up 39% of the total habit mass. This was likely a result of the strong water vapor forcing in the dendritic growth region, the region of maximal ascent typically being associated with the dendritic growth region, the possible optimal overlap of low level moisture supply and high level ice nucleus concentrations, and the depositional advantages of the dendritic crystal structure.

- Cold-type crystals that grow in the middle troposphere were also quite common making up 27% of the total habit mass observed, suggesting the importance of large-scale, baroclinically driven ascent.

- Plate-like and columnar crystals, exhibiting the most basic of shapes, made up a surprisingly small portion of the habit mass.

- For particles with identifiable habit type, rime mass made up 15% of the total mass.

- A habit's rime mass-fraction generally increases as the temperature at which the habit grows gets warmer, due to the absolute increase in available water at those temperatures once water saturation is achieved.

- In keeping with previous studies, crystals that grow at cold temperatures exhibit comparatively little riming, suggesting that lifting aloft is typically not accompanied by strong lifting at low levels

- Graupel-like snow exhibited a rime mass-fraction of 75%.

- Two thirds of all frozen precipitation was the result of deposition, and one third was the result of riming.

4.2 Model Microphysics

Existing bulk microphysics schemes model snow in a simplistic way, retaining a fixed set of physical characteristics, ignoring a particle's specific growth history. Because much of the precipitation reaching the ground in the extratropics originates as snow, improving its behavior in weather models has potentially large implications for quantitative precipitation forecasts. One way of improving snow particle behavior is to allow the conditions it encounters to affect its current and future physical properties. For this reason we explored two alternative methods for doing so, habit prediction and riming prediction.

4.2.1 Habit Prediction

One approach to improving snow's response to its environment is to give the microphysics scheme the ability to track habit mass. This is done by replacing the single prognostic equation for snow's mixing ratio with several prognostic equations, each representing the mixing ratio of a separate habit. With this information, the behavior of snow particles can be adjusted.

We adapted a habit prediction scheme developed by Woods et al. (2007) for use in a bulk microphysics scheme within the WRF model. We then evaluated its effectiveness using data gathered during the observational phase of the present study. Specifically, we compared time series data of crystal type observed during six separate storms to output from model simulations of those same synoptic events. We found that:

- 12 km. and 1.33 km. model simulations behave similarly with respect to the habits produced.

- The habit prediction scheme had difficulty producing needles and especially dendrites when expected, instead producing sectors and columns.

- The cause of the above-described difficulty was not specifically determined, but for a variety of reasons speculated on in the this study, the habit prediction scheme had great difficulty achieving water saturation.

4.2.2 Riming Prediction

A second approach to improving snow's response to its environment is to track rime mass. Much like with habit prediction, this is done by replacing the single prognostic equation for snow's mixing ratio with two prognostic equations, one for the mixing ratio of depositional mass and one for the mixing ratio of rime mass. From this information the behavior of snow particles can be modified accordingly.

We designed and implemented a rime prediction scheme for use within a bulk microphysics scheme within the WRF model. Though special circumstances limited the number of test case simulations that could be run to one, an in depth investigation of the results of rime prediction discovered the following:

- The new mechanism for graupel production delays the formation and fallout of graupel.
- Rimed snow falls faster than unrimed snow.
- Delaying windward graupel fallout and increasing the fall speed of leeward rimed snow appears to result in precipitation being squeezed toward the ridge's crest.
- Increasing riming lowers the mean diameter relative to the control scheme.
- Smaller relative mean diameters reduce relative deposition and sublimation.
- Smaller relative mean diameters increase relative condensation and evaporation through their effect on deposition and sublimation.
- Factors influencing the amount of produced rime include available cloud water and snow, the mean diameter of snow, and possibly the fall velocity of snow.

4.3 Follow Up Work

While many of the goals that were set out for the present study were accomplished, several potential avenues exist for follow up work. The rich observational data set that was obtained over the course of two winters, for example, offers opportunities that could include verifying the behavior of model enhancements developed in this or other studies, or examining the relationship between particle type and size distribution. In addition to working with the observational data set, several experiments could

be performed on the habit prediction scheme that include examining the effect of further increasing model resolution, or tuning the relative humidity threshold acting as the boundary between water supersaturated and subsaturated habit growth regions. Lastly, more exhaustive testing could be done for the riming prediction scheme, which might include running it for longer periods of time, examining it in detail under a variety of orographic and meteorological circumstances, and adjusting the graupel autoconversion threshold value.

BIBLIOGRAPHY

Auer, A. H. and J. M. White, 1982. The combined role of kinematics, thermodynamics and cloud physics associated with heavy snow episodes. *J. Meteor. Soc. Japan*, **60**, 500–507.

Bailey, M. and J. Hallett, 2004. Growth rates and habits of ice crystals between -20 degrees and -70 degrees C. *J. Atmos. Sci.*, **61**, 514–544.

Barthazy, E. and R. Schefolda, 2006. Fall velocity of snowflakes of different riming degree and crystal types. *Atmos. Research*, **82**, 391–398.

Brown, S. R., 1970. *Terminal velocities of ice crystals*. Master's thesis, Colorado State University.

Casson, G. D., 2009. *Evaluating The Importance of Crystal Type on NewSnow Instability*. Master's thesis, University of Washington.

Collins, W. D., P. J. Rasch, B. A. B. J. J. Hack, J. R. McCaa, D. L. Williamson, J. T. Kiehl, B. Briegleb, C. Bitz, S. J. Lin, M. Zhang, and Y. Dai, 2004. Description of the NCAR Community Atmospheric Model (CAM 3.0). Technical note, NCAR. NCAR/TN-464+STR.

Demoz, B. B., R. Zhang, and R. L. Pitter, 1993. An analysis of sierra nevada winter orographic storms: Ground-based ice-crystal observations. *J. Appl. Met.*, **32**, 1826–1836.

Dudhia, J., S. Y. Hong, and K. S. Lim, 2008. A new method for representing mixed-phase particle fall speeds in bulk microphysics parameterizations. *J. Met. Soc. Jap.*, **86A**, 33–44.

Field, P. R. and A. J. Heymsfield, 2003. Aggregation and scaling of ice crystal size distributions. *J. Atmos. Sci.*, **60**, 544–560.

Field, P. R., R. J. Hogan, P. R. A. Brown, A. J. Illingworth, T. W. Choularton, and R. J. Cotton, 2005. Parameterization of ice-particle size distributions for mid-latitude stratiform cloud. *Quart. J. Roy. Meteor. Soc.*, **131**, 1997–2017.

Hallett, J. and S. C. Mossop, 1974. Production of secondary ice particles during the riming process. *Nature,*, **249**, 26–28.

Hanesch, M., 1999. *Fall velocity and shape of snowflakes*. Ph.D. thesis, Swiss Federal Institute of Technology.

Hashino, T. and C. J. Tripoli, 2007. The spectral ice habit prediction system (ships). Part I: Model description and simulation of the vapor deposition process. *J. Atmos. Sci.*, **64**, 2210–2237.

Heymsfield, A. J., 1975. Cirrus uncinus generating cells and the evolution of cirriform clouds. Part I: Aircraft observations of the growth of the ice phase. *J. Atmos. Sci.*, **32**, 799–808.

Hobbs, P. V., 1975. The nature of winter clouds and precipitation in the cascade mountains and their modification by artificial seeding. Part I: Natural conditions. *J. Appl. Met.*, **14**, 783–804.

Hong, S. Y., J. Dudhia, and S. H. Chen, 2004. A revised approach to ice microphysical processes for the bulk parameterization of clouds and precipitation. *Mon. Wea. Rev.*, **132**, 103–120.

Hong, S. Y., Y. Noh, and J. Dudhia, 2006. A new vertical diffusion package with an explicit treatment of entrainment processes. *Mon. Wea. Rev.*, **134**, 2318–2341.

Hong, S. Y. and H. L. Pan, 1996. Nonlocal boundary layer vertical diffusion in a medium-range forecast model. *Mon. Wea. Rev.*, **124**, 2322–2339.

Houze, R. A., 1989. *Cloud Dynamics*. Academic Press.

Houze, R. A., P. V. Hobbs, P. H. Herzegh, and D. B. Parsons, 1979. Size distributions of precipitation particles in frontal clouds. *J. Atmos. Sci.*, **36**, 156–162.

Jr., R. A. H. and S. Medina, 2005. Turbulence as a mechanism for orographic precipitation enhancement. *J. Atmos. Sci.*, **62**, 3599–3623.

Kain, J. S., 2004. The kain-fritsch convective parameterization: An update. *J. Appl. Met.*, **43**, 170–181.

Kajikawa, M., 1989. Observations of the falling motion of early snowflakes. Part II: On the variation of falling velocity. *J. Meteor. Soc. Japan*, **67**, 731–737.

Korolev, A. and G. Isaac, 2003. Roundness and aspect ratio of particles in ice clouds. *J. Atmos. Sci.*, **60**, 1795–1808.

Korolev, A., G. A. Isaac, and J. Hallett, 1999. Ice particle habits in Arctic clouds. *Geophys. Res. Leu.*, **26**, 1299–1302.

Korolev, A., G. A. Isaac, and J. Hallett, 2000. Ice particle habits in stratiform clouds. *Quart. J. Roy. Meteor. Soc.*, **126**, 2873–2902.

Kruger, A. and W. F. Krajewski, 2002. Two-dimensional video disdrometer. A description. *J. Atmos. Oceanic Technol.*, **19**, 602–616.

Lin, Y. L., R. Farley, and H. D. Orville, 1983. Bulk parameterization of the snow field in a cloud model. *J. Clim. And Appl. Met.*, **22**, 1065–1092.

Lo, K. K. and R. E. Passarelli, 1982. The growth of snow in winter storms: An airborne observational study. *J. Atmos. Sci.*, **39**, 697–706.

Locatelli, J. D. and P. V. Hobbs, 1974. Fall speeds and masses of solid precipitation particles. *J. Geophys. Res.*, **79**, 2185–2197.

Lynn, B. H., A. P. Khain, J. Dudhia, D. Rosenfeld, A. Pokrovsky, and A. Seifert, 2005. Spectral (bin) microphysics coupled with a mesoscale model (MM5). Part I: Model description and first results. *Mon. Wea. Rev.*, **133**, 44–58.

Magono, C. and C. W. Lee, 1966. Meteorological classification of natural snow crystals. *J. of the Faculty. of Science*, **II**, 321–335.

Meyers, M. P., R. L. Walko, J. Y. Harrington, and W. R. Cotton, 1997. New rams cloud microphysics parameterization. Part II: The two-moment scheme. *Atmos. Res.*, **45**, 3–39.

Mitchell, D. L., 1988. Evolution of snow-size spectra in cyclonic storms. Part I: Snow growth by vapor deposition and aggregation. *J. Atmos. Sci.*, **45**, 3431–3451.

Mitchell, D. L., R. Zhang, and R. L. Pitter, 1990. Mass-dimensional relationships for ice particles and the influence of riming on snowfall rates. *J. Appl. Met.*, **29**, 153–163.

Mosimann, L., 1995. An improved method for determining the degree of snow crystal riming by vertical doppler radar. *Atmos. Research*, **37**, 305–323.

Nakaya, U., 1954. *Snow Crystals: Natural and Artificial*. Harvard University Press.

Noh, Y., W. G. Cheon, S. Y. Hong, and S. Raasch, 2003. Improvement of the K-profile model for the planetary boundary layer based on large eddy simulation data. *Boundary Layer Met.*, **107**, 401–427.

Power, B. A., P. W. Summers, and J. D'Avignon, 1964. Snow crystal forms and riming effects as related to snowfall density and general storm conditions. *J. Atmos. Sci.*, **21**, 300–305.

Pruppacher, H. R. and J. D. Klett, 1997. *Microphysics of clouds and precipitation*. Springer.

Rauber, R. M., 1987. Characteristics of cloud ice and precipitation during wintertime storms over the mountains of northern colorado. *J. Clim. And Appl. Met.*, **26**, 488–524.

Rauber, R. M. and L. O. Grant, 1986. The characteristics and distribution of cloud water over the mountains of northern colorado during wintertime storms. Part II: Spatial distribution and microphysical characteristics. *J. Clim. And Appl. Met.*, **25**, 489–504.

Rauber, R. M., L. O. Grant, D. Feng, and J. B. Snider, 1986. The characteristics and distribution of cloud water over the mountains of northern colorado during wintertime storms. Part I: Temporal variations. *J. Clim. And Appl. Met.*, **25**, 468–488.

Reisner, J., R. M. Rasmussen, and R. T. Bruintjes, 1998. Explicit forecasting of supercooled liquid water in winter storms using the MM5 mesoscale model. *Quart. J. Roy. Meteor. Soc.*, **124**, 1071–1107.

Rogers, R. R. and M. K. Yau, 1989. *A short course in cloud physics*. Butterworth-Heinemann.

Ryan, B. F., 2000. A bulk parameterization of the ice particle size distribution and the optical properties in ice clouds. *J. Atmos. Sci.*, **57**, 1436–1451.

Saleeby, S. M. and W. R. Cotton, 2008. A binned apporach to cloud-droplet riming implemented in a bulk microphysics model. *J. Appl. Met. and Clim.*, **47**, 694–703.

Sassen, K., A. W. Huggins, A. B. Long, J. B. Snider, and R. J. Meitin, 1990. Investigations of a winter mountain storm in utah. Part II: Mesoscale structure supercooled liquid water development, and precipitation processes. *J. Atmos. Sci.*, **47**, 1323–1350.

Skamarock, W. C., J. B. Klemp, J. Dudhia, D. O. Gill, D. M. Barker, W. Wang, and J. G. Powers, 2005. A description of the advanced research wrf version 2. Technical note, NCAR. NCAR/TN-468+STR.

Smith, R. B., 1979. The influence of mountains on the atmosphere. *Advances in Geophys.*, **21**, 87–230.

Smith, R. B. and I. Barstad, 2004. A linear theory of orographic precipitation. *J. Atmos. Sci.*, **61**, 1377–1391.

Stoelinga, M. T., J. D. Locatelli, and C. P. Woods, 2007. The occurrence of "irregular" ice particles in stratiform clouds. *J. Atmos. Sci.*, **64**.

Straka, J. M. and E. R. Mansell, 2005. A bulk microphysical parameterization with multiple ice precipitation categories. *J. Appl. Met.*, **44**, 445–466.

Super, A. B. and B. A. Boe, 1988. Microphysical effects of wintertime cloud seeding with silver iodide over the rocky mountains. Part III: Observations over the grand mesa, colorado. *J. Appl. Met.*, **27**, 1166–1182.

Thompson, G., P. R. Field, R. M. Rasmussen, and W. D. Hall, 2008. Explicit forecasts of winter precipitation using an improved bulk microphysics scheme. Part II: Implementation of a new snow parameterization. *Mon. Wea. Rev.*, **136**, 5095–5115.

Thompson, G., R. M. Rasmussen, and K. Manning, 2004. Explicit forecasts of winter precipitation using an improved bulk microphysics scheme. Part I: Description and sensitivity analysis. *Mon. Wea. Rev.*, **132**, 519–542.

Vardiman, L., 1978. The generation of secondary ice particles in clouds by crystal-crystal collection. *J. Atmos. Sci.*, **35**, 2168–2180.

Woods, C., 2006. *The Study of Snow Particles in Pacific Northwest Winter Precipitation: Observations and Mesoscale Modeling*. Ph.D. thesis, University of Washington.

Woods, C. P., M. T. Stoelinga, and J. D. Locatelli, 2007. The IMPROVE-1 storm of 1-2 February 2001. Part III: Sensitivity of a mesoscale model simulation to the representation of snow particle types and testing of a bulk microphysical scheme with snow habit prediction. *J. Atmos. Sci.*, **64**.

Yagi, T., 1970. Measurement of the fall velocity of ice crystals drifting in supercooled fog. *J. Meteor. Soc. Japan*, **48**, 487–492.

Young, K. C., 1993. *Microphysical processes in clouds*. Oxford University Press.

Zikmunda, J., 1972. Fall velocities of spatial crystals and aggregates. *J. Atmos. Sci.*, **29**, 1511–1515.